

**DEVELOPMENT OF WATER PURIFICATION
SORBENT FROM PUMICE VOLCANIC ROCK FOR
REMOVAL OF FLUORIDE**

PAUL KIPKOECH KIPRONO

MASTER OF SCIENCE

(Chemistry)

JOMO KENYATTA UNIVERSITY

OF

AGRICULTURE AND TECHNOLOGY

2024

**Development of Water Purification Sorbent from Pumice Volcanic
Rock for Removal of Fluoride**

Paul Kipkoech Kiprono

**A Thesis Submitted in Partial Fulfilment of the Requirements for
the Degree of Master of Science in Chemistry of the Jomo Kenyatta
University of Agriculture and Technology**

2024

DECLARATION

This thesis is my original work and has not been presented for a degree or any other university.

Signature..... Date.....

Paul Kipkoech Kiprono

This thesis has been submitted for examination with our approval as university supervisors.

Signature..... Date.....

Dr. Jackson Kiptoo, PhD

JKUAT, Kenya

Signature..... Date.....

Dr. Elijah Ngumba, PhD

JKUAT, Kenya

Signature..... Date.....

Dr. Eunice Nyawade, PhD

JKUAT, Kenya

DEDICATION

This thesis is dedicated to my wife, Emmily, and daughters Prudence and Precious.

ACKNOWLEDGEMENT

I am grateful to God for providing me with the opportunity to study as well as guidance throughout my studies.

Special thanks to my supervisors, Dr. Kiptoo, Dr. Nyawade, and Dr. Ngumba, for their reviews, guidance, advice, critics, and encouragement that contributed to the success of this research. May God continue to bless you all.

I am obliged to the Chemistry Department for allowing me to study and conduct research in their laboratory. I also thank their laboratory technicians for their assistance and guidance whenever requested.

Dr. Madivoli, Joyline, Amos, and all of my Master of Science in Chemistry classmates, I am grateful for your encouragement and moral support during my studies and research.

Thanks to my colleagues Dr. Kanda, Jeremy, Leakey, Boaz, and Komen for your encouragement throughout my studies.

TABLE OF CONTENTS

| | |
|---|-------------|
| DECLARATION..... | ii |
| DEDICATION..... | iii |
| ACKNOWLEDGEMENTS..... | iv |
| TABLE OF CONTENTS..... | v |
| LIST OF TABLES | x |
| LIST OF FIGURES | xi |
| LIST OF APPENDICES | xii |
| LIST OF PLATES | xiii |
| LIST OF SCHEMES | xiv |
| ABBREVIATIONS AND ACRONYMS | xv |
| ABSTRACT | xvii |
| CHAPTER ONE | 1 |
| INTRODUCTION..... | 1 |
| 1.1 Background of the Study..... | 1 |
| 1.2 Statement of the Problem..... | 3 |
| 1.3 Justification of the Study..... | 3 |
| 1.4 Hypothesis..... | 4 |
| 1.5 Objectives..... | 4 |
| 1.5.1 General Objective..... | 4 |
| 1.5.2 Specific Objectives..... | 4 |

| | |
|---|----------|
| CHAPTER TWO | 5 |
| LITERATURE REVIEW..... | 5 |
| 2.1 Groundwater Pollution | 5 |
| 2.2 Fluoride | 5 |
| 2.2.1 Fluoride Chemistry | 5 |
| 2.2.2 Occurrence of Fluoride | 6 |
| 2.2.3 Benefits and Toxicity of Fluoride | 6 |
| 2.3 Defluoridation Techniques..... | 7 |
| 2.3.1 Coagulation | 8 |
| 2.3.2 Ion-Exchange | 8 |
| 2.3.3 Membrane Filtration..... | 9 |
| 2.3.4 Adsorption..... | 9 |
| 2.4 Adsorbent Materials | 10 |
| 2.4.1 Commercial Activated Carbon..... | 10 |
| 2.4.2 Bone Char | 10 |
| 2.4.3 Agricultural Wastes..... | 11 |
| 2.4.4 Natural Geological Materials | 11 |
| 2.4.5 Aquatic Plants and Materials | 11 |
| 2.5 Silica-Based Adsorbents | 11 |
| 2.5.1 Modification of Silica Surface | 12 |
| 2.5.2 Pumice Volcanic Rock..... | 13 |
| 2.6 Extraction of Silica Nanoparticles | 14 |
| 2.6.1 Hydrolysis of Tetraethyl Orthosilicate (TOES) | 14 |

| | |
|---|-----------|
| 2.6.2 Alkaline Leaching | 15 |
| 2.7 Sorption Isotherms Models | 16 |
| 2.7.1 Freundlich Model | 16 |
| 2.7.2 Langmuir Model..... | 17 |
| 2.8 Kinetic Models | 18 |
| 2.8.1 Pseudo-First-Order Model | 18 |
| 2.8.2 Pseudo-Second-Order Model | 19 |
| 2.9 Techniques | 20 |
| 2.9.1 Ion-Selective Potentiometry..... | 20 |
| 2.9.2 Characterization Techniques | 20 |
| CHAPTER THREE | 23 |
| MATERIALS AND METHODS | 23 |
| 3.1 Study Area..... | 23 |
| 3.2 Samples Collection | 23 |
| 3.3 Instrumentation | 24 |
| 3.4 Chemicals and Reagents | 24 |
| 3.5 Determination of Physico-Chemical Water Quality Parameters | 25 |
| 3.6 Extraction, Modification, and Characterization of Silica Particles..... | 26 |
| 3.6.1 Pretreatment of Pumice Rock..... | 26 |
| 3.6.2 Extraction of Silica Particles (SPs) from Pumice Rock | 26 |
| 3.6.3 Characterization | 27 |
| 3.7 Batch Adsorption Studies..... | 28 |
| 3.7.1 Optimization of pH | 28 |

| | |
|--|-----------|
| 3.7.2 Optimization of Sorbent Dose..... | 29 |
| 3.7.3 Optimization of Contact Time | 29 |
| 3.7.4 Optimization of Initial Fluoride Concentration..... | 29 |
| 3.7.5 Adsorption Isotherms and Kinetic Models | 29 |
| 3.8 Removal of Fluoride from Real Water Samples | 30 |
| 3.9 Regeneration Studies..... | 30 |
| CHAPTER FOUR..... | 31 |
| RESULTS AND DISCUSSION | 31 |
| 4.1 Physico-Chemical Water Quality Parameters | 31 |
| 4.2 Fluoride Levels..... | 36 |
| 4.2.1 Statistical Correlation Analysis..... | 37 |
| 4.3 Extraction, Modification, and Characterization of Silica Particles..... | 39 |
| 4.3.1 Silica Yield..... | 39 |
| 4.3.2 Characterization | 40 |
| 4.4 Adsorption Studies | 44 |
| 4.4.1 Effect of pH..... | 44 |
| 4.4.2 Effect of sorbent dose..... | 46 |
| 4.4.3 Effect of Contact Time..... | 47 |
| 4.4.4 Effect of Initial Fluoride Concentration | 47 |
| 4.4.5 The Effect of Modification of Silica Particles with Iron on Fluoride Removal..... | 48 |
| 4.4.6 Adsorption Isotherms | 50 |
| 4.4.7 Kinetics of Defluoridation | 52 |

| | |
|--|-----------|
| 4.5 Application of FMSPs to Real Water Samples | 55 |
| 4.6 Regeneration Studies..... | 55 |
| CHAPTER FIVE..... | 57 |
| CONCLUSIONS AND RECOMMENDATIONS..... | 57 |
| 5.1 Conclusions | 57 |
| 5.2 Recommendations | 58 |
| REFERENCES..... | 59 |
| APPENDICES | 72 |

LIST OF TABLES

| | |
|--|----|
| Table 4.1: Results for Onsite Analysis, Alkalinity, and Hardness (n = 3) | 32 |
| Table 4.2: Concentrations of Major Ions (n = 3) | 34 |
| Table 4.3: Statistical Correlation Matrix for Physico-Chemical Parameters | 38 |
| Table 4.4: Recovery of Silica Particles from Pumice Rock (n = 3) | 39 |
| Table 4.5: Chemical Composition of Pumice Rock, SPs, and FMSPs | 41 |
| Table 4.6: Calculated Freundlich and Langmuir Isotherm Parameters..... | 51 |
| Table 4.7: Kinetics Models Constants | 53 |
| Table 4.8: Comparison of Efficiency of FMSPs with Different Adsorbents | 54 |

LIST OF FIGURES

| | |
|---|----|
| Figure 2.1: Amorphous Silica Structure | 12 |
| Figure 3.1: Location of Paka Volcano and Boreholes in Tiaty, Baringo in Kenya. . | 23 |
| Figure 4.1: Fluoride Levels in Borehole Water | 36 |
| Figure 4.2: The Correlation between Fluoride and pH for Fluoride-Rich Boreholes | 38 |
| Figure 4.3: Diffractograms of (a) Pumice Rock, (b) SPs, and (c) FMSPs..... | 42 |
| Figure 4.4: FTIR Spectra of Pumice Rock (a), SPs (b), and FMSPs (c) | 43 |
| Figure 4.5: SEM Micrograph for Extracted Silica Particles | 44 |
| Figure 4.6: Effect of pH on the Adsorption Capacity of FMSPs..... | 45 |
| Figure 4.7: Effect of Sorbent Dose on the Adsorption Capacity of FMSPs | 46 |
| Figure 4.8: Effect of Contact Time on the Adsorption Capacity of FMSPs..... | 47 |
| Figure 4.9: Effect of Initial Concentration on the Sorption Capacity of FMSPs..... | 48 |
| Figure 4.10: Effect of Modifying Silica Particles with Iron on Fluoride Removal .. | 49 |
| Figure 4.11: Freundlich Isotherm Plot for Defluoridation Using FMSPs..... | 50 |
| Figure 4.12: Langmuir Isotherm Plot for Defluoridation Using FMSPs | 51 |
| Figure 4.13: Pseudo-First-Order Kinetics Plot for Defluoridation Using FMSPs.... | 52 |
| Figure 4.14: Pseudo-Second-Order Kinetics Plot for Defluoridation Using FMSPs | 53 |
| Figure 4.15: Comparison of Fluoride Levels in Raw and Treated Groundwater | 55 |
| Figure 4.16: Regeneration of Fe-Modified Silica Particles (FMSPs)..... | 56 |

LIST OF APPENDICES

| | |
|---|----|
| Appendix I: Standard Calibration Curve for Sodium | 72 |
| Appendix II: Standard Calibration Curve for Potassium | 73 |
| Appendix III: Standard Calibration Curve for Calcium..... | 74 |
| Appendix IV: Standard Calibration Curve for Magnesium..... | 75 |
| Appendix V: Standard Calibration Curve for Sulphate | 76 |
| Appendix VI: Standard Calibration Curve for Fluoride | 77 |
| Appendix VII: Percent Fluoride Removal at Different pH | 78 |
| Appendix VIII: Percent Fluoride Removal at Different Sorbent Doses | 79 |
| Appendix IX: Percent Fluoride Removal at Different Contact Times | 80 |
| Appendix X: Percent Fluoride Removal at Different Initial Concentrations..... | 81 |
| Appendix XI: Effect of Modification of SPs with Iron on Fluoride Removal | 82 |
| Appendix XII: Freundlich Isotherm Raw Data at Optimum Conditions..... | 83 |
| Appendix XIII: Langmuir Isotherm Raw Data at Optimum Conditions..... | 84 |
| Appendix XIV: Pseudo-First-Order Kinetics Raw Data at Optimum Conditions ... | 85 |
| Appendix XV: Pseudo-Second-Order Kinetics Raw Data at Optimum Conditions. | 86 |
| Appendix XVI: Publication | 87 |

LIST OF PLATES

Plate 2.1: Pumice Rock 14

LIST OF SCHEMES

| | |
|---|----|
| Scheme 2.1: Synthesis Path Way of Silica Nanoparticles..... | 14 |
| Scheme 2.2: Condensation of Silicic Acid to form a Network of Silica Gel | 15 |

ABBREVIATIONS AND ACRONYMS

| | |
|---------------|--|
| APHA | American Public Health Association |
| EBT | Eriochrome Black T |
| EC | Electrical Conductivity |
| EDTA | Ethylenediaminetetraacetic acid |
| FMSPs | Fe-Modified Silica Particles |
| FTIR | Fourier Transform Infrared |
| HDPE | High-Density Polyethylene |
| HDTMA | Hexadecyltrimethylammonium |
| HSAB | Hard and Soft Acids and Bases |
| ISE | Ion Selective Electrode |
| NF | Nanofiltration |
| RO | Reverse Osmosis |
| SEM | Scanning Electron Microscope |
| SDG | Sustainable Development Goal |
| SNPs | Silica Nanoparticles |
| SPs | Silica Particles |
| TDS | Total Dissolved Solids |
| TISAB | Total Ionic Strength Adjustment Buffer |
| UNICEF | United Nations International Children's Emergency Fund |
| UV-Vis | Ultraviolet - Visible |
| WHO | World Health Organization |

XRD X-ray Diffraction

XRF X-ray Fluorescence

ABSTRACT

Groundwater is extensively used for household purposes in Kenya's Rift Valley, particularly in drought-prone regions such as Tiaty, Baringo County. However, groundwater often contains harmful geogenic pollutants such as fluoride. Majority of conventional defluoridation techniques while effective, they are costly and complicated to operate. Hence, there is a need to develop simple and low-cost adsorbents using locally available materials for fluoride remediation. In this study, a silica-based defluoridation sorbent was developed from pumice rock obtained from the Paka volcano in Baringo County, Kenya. Alkaline leaching technique was used to extract silica particles from pumice rock, which was subsequently modified with iron to enhance its affinity for fluoride. To assess its efficacy, randomly sampled borehole water was used. Temperature, electrical conductivity (EC), total dissolved solids (TDS) and pH were determined onsite using a portable multi-parameter meter. Fluoride and sulphate levels were determined using potentiometry and turbidimetry, respectively. Flame photometry was used to determine potassium and sodium. Calcium and magnesium were analyzed using flame atomic absorption spectrophotometry. Bicarbonates, chloride, alkalinity, and hardness levels were determined using titrimetry. The scanning electron microscopy, X-ray diffraction, Fourier transform infrared and X-ray fluorescence spectroscopy were used to characterize the sorbent. Batch experiments were used to determine the optimal pH, sorbent dose, and contact time for fluoride removal. Temperature, pH, EC, and TDS were in the range, 27.4 - 40.7 °C, 6.8 - 8.7, 402.89 - 4212.99 $\mu\text{S}/\text{cm}$, and 201.24 - 2111.77 mg/L, respectively. The levels of major ions were in the range, HCO_3^- (127.1 - 1453.2 mg/L), Na^+ (46.81 - 856.37 mg/L), Cl^- (19.85 - 288.02 mg/L), SO_4^{2-} (15.62 - 95.31 mg/L) Mg^{2+} (1.38 - 29.41 mg/L), Ca^{2+} (1.73 - 30.84 mg/L), K^+ (6.08 - 26.49 mg/L) and F^- (0.88 - 16.4 mg/L). The extracted silica particles were 96.71 % pure and amorphous, whereas the iron-functionalized silica particles contained 93.67 % SiO_2 and 2.93 % Fe_2O_3 . The optimal pH, sorbent dose, and contact time for defluoridation using initial fluoride concentration of 20 mg/L were 6, 1 g, and 45 minutes, respectively. Defluoridation fitted the Freundlich's isotherm model ($R^2 = 0.989$), indicating multilayer adsorption on a heterogeneous surface, and it followed pseudo-second-order kinetics ($R^2 = 0.992$), implying chemisorption. Fluoride levels in borehole water decreased significantly upon defluoridation; Intex 4.57 - 1.1 (75.27 %), Kadokoi 2.46 - 0.54 (78.05 %), and Naudo 5.39 - 1.2 mg/L (77.74 %). The Fe-modified silica sorbent has been demonstrated to significantly remove fluoride from water samples. Hence, it can be used as a mitigation strategy against the adverse health effects associated with elevated fluoride levels in drinking water.

CHAPTER ONE

INTRODUCTION

1.1 Background of the Study

Groundwater is the most easily accessible source of drinking water, but it is also the most polluted, posing a health risk. The World Health Organization (WHO) attributes 80 % of all diseases worldwide to poor water quality (Vijila *et al.*, 2021). Today one in every three people worldwide lack access to safe drinking water due to pollution, yet the Global Sustainable Development Goal 6 (SDG-6) aims to achieve universal access to safe drinking water and sanitation by 2030 (WHO & UNICEF, 2021). Fluoride is one of the water pollutants commonly found in untreated groundwater but is also essential in the body as a trace element for the development of teeth and bones (Gai & Deng, 2021; Vinati *et al.*, 2015). Prolonged exposure to high fluoride levels can cause dental and skeletal fluorosis, as well as harm to the kidneys, liver, brain, and thyroid glands (Wambu *et al.*, 2016; Wan *et al.*, 2021). Over 260 million people worldwide are exposed to high fluoride levels through groundwater in East Africa's Rift Valley, Asia, Europe, and America (Kebede *et al.*, 2016; Kimambo *et al.*, 2019; Sharma *et al.*, 2021). This has been attributed to geogenic processes such as volcanic activities and weathering of fluoride-rich minerals (Fuoco *et al.*, 2021; Olaka *et al.*, 2016).

Fluoride enrichment in groundwater is also aided by effluents from the fertilizer, ceramic, pesticide, glass, aluminium and refrigerant industries (Rafique *et al.*, 2013; Sadhu *et al.*, 2022). The World Health Organization (WHO) has established a fluoride threshold of 1.5 mg/L in drinking water (WHO, 2017), hence defluoridation processes such as ion exchange, adsorption, coagulation, precipitation and reverse osmosis are crucial to maintaining fluoride levels within this limit (Wan *et al.*, 2021). However, most of these techniques are expensive to maintain and operate. Another constraint is the production of toxic sludge through methods such as precipitation, coagulation, and membrane filtration. Furthermore, techniques such as reverse osmosis and ion exchange are complicated and expensive. These constraints have

necessitated the need for more research on the use of adsorbents to defluoridate water (Gisi *et al.*, 2016; Pan *et al.*, 2019).

Adsorption is the most preferred water purification technique because it is cheap, efficient, does not generate sludge, is simple to operate, and does not need electric power or specialized skills to operate. In addition, the adsorbents can be regenerated and reused making them the best at the household level and in small communities in less developed rural areas (Ahmadijokani *et al.*, 2021). Commercial activated carbon derived from coal is among the most effective adsorbents for fluoride removal from water. It has a high specific surface area and is highly porous, however, it is extremely expensive and has regeneration difficulties (Gisi *et al.*, 2016). Other effective materials include bauxite (Cherukumilli *et al.*, 2018), bone char, metal oxides, polymer materials, biosorbents (Nehra *et al.*, 2020), agricultural wastes (Wan *et al.*, 2021), sea materials, fly ash, carbonaceous materials (He *et al.*, 2020), nanoparticles (Ghosh *et al.*, 2022) and geomaterials (Asgari *et al.*, 2012), all of which are low in cost and readily available, as is the case of silica mineral (SiO₂).

Silica is an auspicious material with distinct features that satisfy almost all of the selection criteria for an ideal water purification adsorbent, such as chemical inertness, structural and thermal stability, high specific surface area, non-toxicity, and large pore size (Diagboya & Dikio, 2018). Furthermore, it is abundant and widely distributed in nature, particularly in volcanic rocks such as pumice (60-70 %) (Mohseni-Bandpei *et al.*, 2020; Soleimani *et al.*, 2019). Silica surface has functional groups (-Si-OH and -Si-O-Si-) that are readily modified to increase adsorption capacity and enhance selectivity towards a target pollutant. Modification has been previously achieved by functionalization with organic groups, coating with metal oxides, or doping with metal ions (Diagboya & Dikio, 2018). Wang *et al.* (2018) used amino-functionalized silica particles for heavy metals removal from water, and the high sorption capacity was attributed to strong coordination between amino groups on the silica surface with metal ions. In another study, Zhang *et al.* (2019) utilized iron oxide-coated silica particles for the removal of organic pollutants from water. Iron oxide coating provides additional binding sites for the pollutants, enhancing the removal efficiency. In this study, silica-based defluoridation sorbent

was prepared by isolating silica particles from pumice volcanic rock. Its surface was then modified with iron to increase sorption capacity due to its high affinity for fluoride ions and its ability to form strong complexes with fluoride. In addition, iron is non-toxic and abundant in nature. Batch experiments were used to evaluate the kinetics and isotherm of fluoride adsorption, as well as the effects of pH, contact time, dosage and initial concentration on fluoride removal. The efficacy of the adsorbent was then evaluated using borehole water samples.

1.2 Statement of the Problem

Access to sustainable safe drinking water remains a challenge for nearly 780 million people across the globe, with 50 % relying on groundwater that is often polluted with natural pollutants such as fluoride (WHO & UNICEF, 2021). Consequently, managing groundwater pollution is critical. The quality of water for household use is defined by its chemical constituents as well as their concentrations. Fluoride is a harmful pollutant often found naturally in underground water sources and has affected over 250 million people globally in countries such as Tanzania, Kenya and Ethiopia all within the East African Rift Valley System (Kimambo *et al.*, 2019). This has resulted in adverse health effects such as osteoporosis and fluorosis. The WHO has established a fluoride threshold of 1.5 mg/L in drinking water. Most of the conventional defluoridation techniques such as ion-exchange and reverse osmosis though effective, they are complicated and costly to acquire. Hence, there is a need for defluoridation using low-cost adsorbents that are efficient, simple to operate, readily available, and can be easily regenerated with minimal sludge production.

1.3 Justification of the Study

There is an urgent need to remove fluoride, which is commonly found in groundwater around the world and has been linked to adverse health effects. Adsorption is the most ideal technique for the removal of fluoride from water due to its ease of operation, cost-effectiveness, environmental friendliness, simplicity of design and availability of a diverse range of adsorbents that can be regenerated, reused and chemically modified to enhance the selective affinity of a pollutant. However, most adsorbents in use today are ineffective in fluoride mitigation due to

flaws such as low specific surface area, low affinity for fluoride ions, low porosity, regeneration difficulties, and low adsorption capacity. Thus, the development of economical and effective adsorbents with high adsorption capacity and ease of regeneration for the efficient removal of fluoride from water remains a challenge that demands continued research. Silica is an auspicious material with distinct features that satisfy almost all of the selection criteria for an ideal water purification adsorbent. Furthermore, it is abundant in nature, and its extraction is simple and economical, rendering it superior to many other adsorbents. In this study, a silica-based defluoridation sorbent was developed using pumice, a silica-rich volcanic rock found in abundance along Kenya's Rift Valley.

1.4 Hypothesis

Fe-modified silica particles (FMSPs) cannot significantly remove fluoride from water.

1.5 Objectives

1.5.1 General Objective

To develop a water purification sorbent from pumice volcanic rock for the removal of fluoride.

1.5.2 Specific Objectives

- i. To determine selected physico-chemical water quality parameters of borehole water samples collected from Tiaty, Baringo County in Kenya.
- ii. To extract, modify, and characterize silica particles from pumice volcanic rock obtained from Tiaty, Baringo County in Kenya.
- iii. To optimize sorption parameters such as pH, sorbent dose, contact time and initial concentration for the removal of fluoride using Fe-modified silica particles (FMSPs).
- iv. To determine the efficiency of Fe-modified silica particles (FMSPs) in the removal of fluoride from borehole water samples collected from Tiaty, Baringo County in Kenya.

CHAPTER TWO

LITERATURE REVIEW

2.1 Groundwater Pollution

Groundwater pollution is regarded as an undesirable change in the physical, chemical, and biological properties of the groundwater. Physical properties include temperature, color, turbidity, taste, and odor. Water can be contaminated biologically by the presence of pathogens like bacteria, viruses, algae, and protozoa. Inorganic water pollutants are substances such as lead, arsenic, cyanide, fluoride, and mercury. Organic contaminants include pesticides, dyes, insecticides, paints, solvents, medicine, and disinfectants among others. Radiological pollution of water is caused by radioactive elements such as U^{226} , Ra^{226} , Ra^{228} , and Rn^{228} (Hasan *et al.*, 2019). Groundwater pollution is a result of natural processes such as aquifer mineral dissolution, volcanic activities, and weathering, as well as anthropogenic activities such as mining and agriculture. Drinking contaminated groundwater has negative health implications for humans and animals, necessitating the adoption of an effective water filtration system (Rasool *et al.*, 2015).

2.2 Fluoride

2.2.1 Fluoride Chemistry

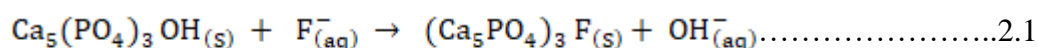
Fluoride is an anion of fluorine, that is classified as a halogen element in the periodic table. Fluorine is the 13th most abundant element constituting 0.1 % of the earth's crust (Kut *et al.*, 2016). Fluorine is a greenish diatomic and highly corrosive gas (Biswas *et al.*, 2017). It is a very reactive and the most electronegative element in the periodic table. For this reason, it cannot be found in its elemental state in nature (Jagtap *et al.*, 2012). Due to the small ionic radius of fluoride ion, it acts like a ligand and can form several organic and inorganic compounds in air, rock, soil, minerals, water, and living organisms (Habuda-Stanić *et al.*, 2014).

2.2.2 Occurrence of Fluoride

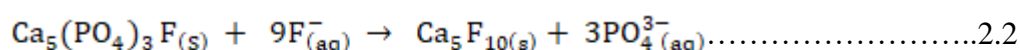
Fluoride gets into the human body via sources such as cosmetics, medicine, drinking water, and food. However, drinking water is the principal source (Akafu *et al.*, 2019). Elevated fluoride in groundwater is mainly due to weathering and dissolution of fluoride-rich minerals, ores, and rocks in the aquifers such as amphiboles, mica, cryolite (Na₃AlF₆), fluor spar (CaF₂), sellaite (MgF₂), and fluorapatite (Ca₅(PO₄)₃F) (Akafu *et al.*, 2019; Tomar *et al.*, 2013). Fluoride and hydroxyl ions co-exist in these minerals and are capable of ion exchange due to similarities in their charge and ionic radius of 1.36 Å and 1.40 Å respectively (Brahman *et al.*, 2013; Ganvir & Das, 2011). Fluoride effluents can be released from industries into the environment either in gaseous (e.g., HF, F₂, SiF₄, and H₂SiF₄) or particulate forms (CaF₂, NaF, and Na₂SiF₆). Anthropogenic sources such as improper disposal of industrial effluents, fertilizers, pesticides, glass manufacturing, aluminum manufacturing, and wood preservatives are also responsible for high levels of fluoride in soil and groundwater (Alkurdi *et al.*, 2019; Kimambo *et al.*, 2019).

2.2.3 Benefits and Toxicity of Fluoride

Fluoride is both harmful and beneficial depending on the dose and duration of exposure (Cai *et al.*, 2015). A fluoride concentration of 1.5 mg/L is the maximum allowable limit for fluoride in drinking water (WHO, 2017). Below 1.5 mg/L, it is critical for skeletal and dental development, where it substitutes the hydroxyl group in hydroxyapatite to form harder fluorapatite (Equation 2.1) (Kimambo *et al.*, 2019).



Excess fluoride causes the conversion of hydroxyapatite to fluorapatite to go beyond the hydroxyl group resulting in denser and brittle teeth and bones (Equation 2.2), a condition referred to as fluorosis (Mohapatra *et al.*, 2009).



Dental fluorosis arises from fluoride exposure in the range of 1.5-4 mg/L (Malago *et al.*, 2017). A dose beyond 4 mg/L for a prolonged period during childhood can result in skeletal fluorosis signified by difficulty in walking as a result of permanent bones and joint deformity (Cai *et al.*, 2015; Tomar *et al.*, 2014). Fluoride can also cause arthritis, infertility, and osteoporosis as well as harm organs such as the kidney, thyroid gland, liver, endocrine, and brain (Lin *et al.*, 2016; Tomar *et al.*, 2013). More than 260 million people worldwide have been affected by skeletal and dental fluorosis (Olaka *et al.*, 2016). Countries within the East Africa Rift Valley System including Kenya, Ethiopia, and Tanzania have reported elevated fluoride levels in groundwater attributed to volcanic rocks and active volcanoes. In Kenya, this is correlated with cases of skeletal and dental fluorosis in places such as Nakuru, Naivasha, and Baringo (Alkurdi *et al.*, 2019). To mitigate the above health situations, the WHO recommended the limit of fluoride in drinking water from 0.5 to 1.5 mg/L (WHO, 2017). To attain this regulation an efficient and affordable water treatment system is needed.

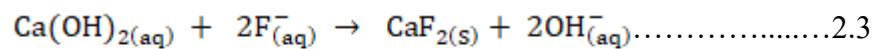
2.3 Defluoridation Techniques

Fluoride can be removed from water by conventional techniques such as adsorption, reverse osmosis, coagulation, Ion exchange, membrane filtration, chemical precipitation, and electrodialysis (Thakur & Mondal, 2017). The choice of these techniques depends on factors such as costs, the nature of the pollutant, the concentration of fluoride, the handling of residue, and the versatility of the method (Velazquez-jimenez *et al.*, 2015). The major challenge with the most of these techniques is maintenance and operation costs. Another limitation is the generation of toxic sludge by methods like precipitation, coagulation, and membrane filtration. In addition, techniques like reverse osmosis and ion exchange are complicated and quite expensive hence, the adoption of water adsorbents (Gisi *et al.*, 2016). Adsorption is the most preferred water purification technique because it is cheap, efficient, does not generate sludge, is simple to operate, and does not need electric power or specialized skills to operate. In addition, the adsorbents can be regenerated and reused making them the best at the household level and in small communities in less developed rural areas (Ahmadijokani *et al.*, 2021).

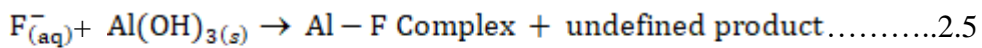
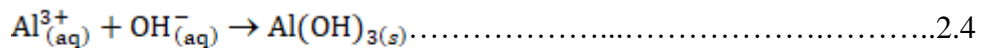
2.3.1 Coagulation

This is a chemical process where fluoride is removed from water through precipitation using appropriate precipitating agents. Lime and alum ($\text{Al}_2(\text{SO}_4)_3 \cdot 18\text{H}_2\text{O}$) are commonly used. Lime dosing is the first step, which causes

fluoride to precipitate as calcium fluoride (Equation 2.3) and raises the pH of water to 11-12.



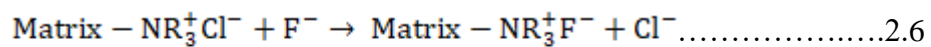
Alum is then added to cause coagulation via two reactions. First, it reacts with hydroxyl ions to form insoluble aluminium hydroxide (Equation 2.4) which then reacts with fluoride ions present in water, as described in Equation 2.5 (Kut *et al.*, 2016).



2.3.2 Ion-Exchange

In this method, fluoride is removed from water using ion exchange resins containing quaternary ammonium functional groups ($-\text{NR}_3^+\text{Cl}^-$). The mechanism of fluoride

removal is the substitution of chloride ions in the resin with fluoride ions as illustrated in Equation 2.6 (Wan *et al.*, 2021).



The process progresses until all the active ion exchange sites are fully occupied. To regenerate the resin, it is washed with water supersaturated with sodium chloride. Through this, the chloride ions are replaced with fluoride ions. Fluoride ions substitute chloride ions since it is more electronegative than chloride (Velazquez-jimenez *et al.*, 2015).

2.3.3 Membrane Filtration

This process utilizes a semi-permeable membrane between adjacent phases that serve as a barrier for pollutants. Reverse osmosis (RO), nanofiltration (NF), dialysis, and electro dialysis are examples of this technique. The efficiency of defluoridation of water by membrane filtration is up to 98 % (Meenakshi and Maheshwari, 2006; Sadegh *et al.*, 2017). Reverse osmosis is a physical process whereby raw water is passed through a semipermeable membrane under pressure. It is the opposite of natural osmosis since the pressure is applied to the concentrated region to overcome the natural osmotic pressure (Jagtap *et al.*, 2012). The principle of nanofiltration is similar to reverse osmosis. However, in NF the membrane pores are relatively larger than those in RO. This reduces flow resistance to both solutes and solvents. NF uses low pressure and removes mostly larger dissolved solids as compared to RO. In contrast, RO operates with high pressure and removes entirely all dissolved solids (Meenakshi & Maheshwari, 2006; Mohapatra *et al.*, 2009). In electro dialysis, an ion-exchange membrane is used to remove ionic contaminants from water under the influence of an electric field, whereas, in dialysis, solutes are transported from one solution to another across a membrane as a result of a concentration gradient, rather than retaining a solute on the membrane while water percolates through it, as in nanofiltration (NF) and reverse osmosis (RO) (Mohapatra *et al.*, 2009).

2.3.4 Adsorption

Adsorption is a mass transfer process whereby a pollutant is isolated from water by accumulation on a solid or liquid surface. The adsorption can either be physisorption or chemisorption depending on the nature of the interaction between adsorbate and adsorbent. Chemisorption occurs if the forces of attraction between the adsorbate and adsorbent surface are strong due to chemical bonding such as covalent or ionic

bonding with a monolayer of adsorbate on the adsorbent surface. However, if the force of attraction is due to weak Van der Waals forces with multilayers of adsorbate on the adsorbent surface, the process becomes physisorption and is usually reversible (Aregu *et al.*, 2018; Gisi *et al.*, 2016; Sadegh *et al.*, 2017).

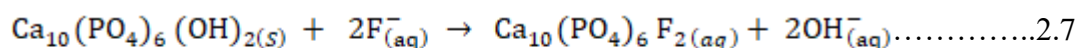
2.4 Adsorbent Materials

2.4.1 Commercial Activated Carbon

The most effective commercial adsorbent material for removing a wide range of contaminants from water is activated carbon derived from coal. The adsorbent is extremely porous with a high specific surface area. However, the high cost of coal-based activated carbon and its regeneration difficulties have restricted its extensive usage (Gisi *et al.*, 2016). This has necessitated a shift to low-cost and readily available alternative materials like industrial wastes, agricultural waste, sea materials, and natural geological materials.

2.4.2 Bone Char

Bone charcoals are blackish porous low-cost adsorbents derived from burned and ground animal bones. The bones are usually packed in columns or buckets then water is passed through them. Bone char can effectively remove fluoride from water. However, poorly prepared bone char results in an unpleasant taste, odor, and color in purified water. The removal of fluoride ion (F⁻) from water is due to the hydroxyl group (OH⁻) in hydroxyapatite (Ca₁₀(PO₄)₆(OH)₂). Ion exchange is the key mechanism for removal due to the high affinity of fluoride ions to replace the hydroxyl group as illustrated in Equation 2.7 (Alkurdi *et al.*, 2019).



2.4.3 Agricultural Wastes

Agricultural solid wastes are also classified as cheap and readily available adsorbents. The ability of plant material to remove pollutants is due to the presence of functional groups such as hydroxyl (-OH), carboxyl (-COOH), and amine (-NH₂) in the basic components of plants such as hemicellulose, lignin, proteins, simple sugars, lipids and starch (Gisi *et al.*, 2016). Fluoride removal has been investigated using rice husks loaded with aluminium hydroxide (Ganvir & Das, 2011).

2.4.4 Natural Geological Materials

Clays and zeolites are some low-cost natural geological materials that have been used as adsorbents. Clays have got large surface area and negative charge on the silicate mineral which makes them have high adsorption capabilities. The negative charge can be neutralized by a positively charged adsorbate or can be modified by a cationic surfactant to attract a negatively charged adsorbate (Gisi *et al.*, 2016). Zeolites consist of aluminosilicate minerals with interlinked alumina and silica moieties. The adsorption capabilities of zeolite are due to its good ion exchange properties and large surface area (Renu *et al.*, 2017). Fluoride removal has been investigated using clay minerals (Vinati *et al.*, 2015).

2.4.5 Aquatic Plants and Materials

Chitosan and hyacinth are examples of low-cost adsorbents derived from water bodies. Chitosan is a naturally occurring polysaccharide derivative obtained from crustaceans, it contains hydroxyl and amino groups responsible for adsorption through chelates formation (Renu *et al.*, 2017). Fluoride removal has been investigated using hyacinth, an aquatic plant coated with aluminium and iron oxide (Murambasvina & Mahamadi, 2020).

2.5 Silica-Based Adsorbents

Silica is among the most abundant elements on the earth's crust and it is present in entirely every mineral. Silica-based adsorbents are gaining interest in water treatment since they fulfill the criteria for selection of adsorbents such as; chemical inertness,

non-toxic, low-cost, non-corrosive, thermally stable, mechanically stable, large pore size, and high adsorption capacity due to very high specific surface (Diagboya & Dikio, 2018). In addition, silica surface has two functional groups (Figure 2.1); silanol (-Si-OH) and siloxane (-Si-O-Si-) that can be modified with organic or inorganic chemical groups to increase selectivity towards specific pollutants (Bilici & Pala, 2011).

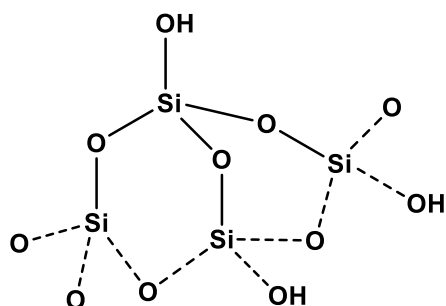


Figure 2.1: Amorphous Silica Structure

2.5.1 Modification of Silica Surface

Silica fulfills most of the criteria for the selection of adsorbent for the removal of pollutants from water. However, modification of its surface is often necessary to enhance its adsorption capacity, selectivity, and stability. Modification can be achieved via approaches such as functionalization with organic groups, coating with metal oxides, doping with metal ions, or coating with a polymers (Diagboya & Dikio, 2018). Wang *et al.* (2018) used amino-functionalized silica particles for heavy metals removal from water, and the high sorption capacity was attributed to strong coordination between amino groups on the silica surface with metal ions. Zhang *et al.* (2019) utilized iron oxide-coated silica particles for the removal of organic pollutants from water. Iron oxide coating provided additional binding sites for the pollutants, enhancing the removal efficiency. Mesoporous silica nanoparticles functionalized with chitosan derived from mushrooms resulted in selective and high fluoride removal efficiency of 95 %, with a maximum sorption capacity of, 58.8 mg/g (Srivastava *et al.*, 2020). Pillai and Pandian, (2020) used rice husks derived silica nano doped on calcium peroxide for the removal of fluoride from water, and a high defluoridation efficiency of 94 % was achieved, with a maximum adsorption

capacity of 55 mg/g. This was attributed to increased surface area by calcium peroxide (CaO₂). Zeolite, a silica-rich material was synthesized from kaolin clay and then modified with aluminium sulphate for defluoridation. A higher fluoride adsorption efficiency of 98.87 % was reported. This was attributed to zeolite's large surface area and high porosity (Tabi *et al.*, 2021).

2.5.2 Pumice Volcanic Rock

Pumice is an igneous volcanic rock that is silica-rich (Mohseni-Bandpei *et al.*, 2020; Soleimani *et al.*, 2019). It has a high porosity of up to 85 % and is formed during violent volcanic eruptions when gas-rich lava solidifies (Asgari *et al.*, 2012; Heibati *et al.*, 2014). Pumice rocks are found in bulk along the Rift Valley System where explosive eruptions occur in centralized volcanic centers (Sekomo *et al.*, 2012). In Kenya, these volcanic centers include; Barrier, Namanuru, Emuruangogolak, Silali, Paka, Korosi, Menengai, Longonot, and Suswa craters (Simiyu, 2010). Studies have been done to evaluate the adsorption capacity of pumice rock, being a low-cost, non-toxic, and naturally available by-product of volcanic eruption, for instance; surface

modified pumice with a cationic surfactant, hexadecyltrimethylammonium (HDTMA) removed 96 % of fluoride from water at pH 6 for 30 minutes with a dose of 0.5 gL⁻¹ (Asgari *et al.*, 2012). A study by Salifu *et al.*, (2013) utilized pumice rock coated with aluminum hydroxide for the removed of fluoride from water. The fluoride levels reduced from an initial concentration of 5 mgL⁻¹ to below the WHO limit of 1.5 mgL⁻¹ in 1 hour with a dose of 10 mg/L. To increase the adsorption capacity of pumice rock, silica nanoparticles can be extracted from it since they have high reactivity and large surface area compared to bulk particles more so they can be functionalized easily to increase their affinity towards a target pollutant. Hence, silica can be obtained from pumice volcanic rock (Plate 2.1) for the preparation of silica nanoparticles.

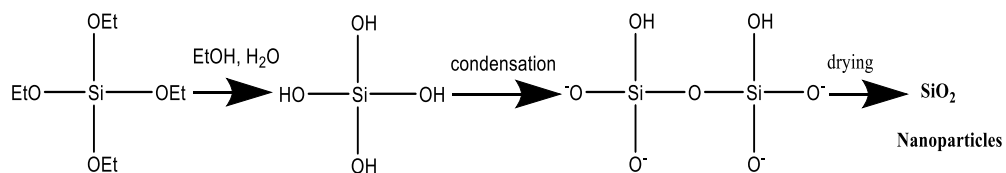


Plate 2.1: Pumice Rock

2.6 Extraction of Silica Nanoparticles

2.6.1 Hydrolysis of Tetraethyl Orthosilicate (TOES)

Stober was the first to synthesize silica nanoparticles (SNPs), by use of tetraethyl orthosilicate (TOES) as the silica precursor (Stober & Fink, 1967). This is illustrated by the synthesis path way in Scheme 2.1 (Karande *et al.*, 2021).

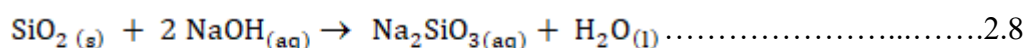


Scheme 2.1: Synthesis Path Way of Silica Nanoparticles

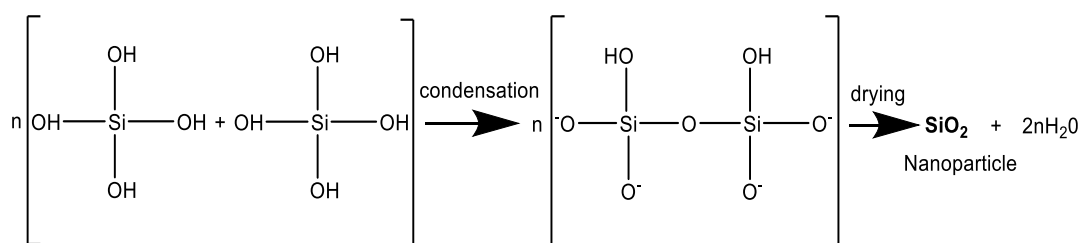
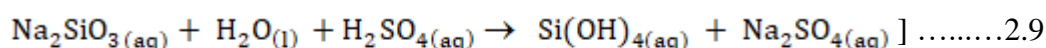
Later, silica precursors such as silicon alkoxide and Na_2SiO_3 were also used to synthesize silica nanoparticles on a massive scale (Zulfiqar *et al.*, 2016). In this protocol, sand is reduced by carbon at over 1000 °C to yield silicon alkoxide, whereas Na_2SiO_3 solution is recovered from quartz using Na_2CO_3 at elevated temperature. These operations are both costly and environmentally unfriendly as they consume a lot of power and generate a lot of greenhouse gases such as CO_2 . Consequently, studies on low-cost excellent silica sources such as bentonites (Zulfiqar *et al.*, 2016), pumice rock (Mourhly *et al.*, 2015) fly ash, sugarcane bagasse (Rovani *et al.*, 2018), and rice husks ash (Nayak & Datta, 2021) have been investigated, with extraction processes that are both economical and eco-friendly.

2.6.2 Alkaline Leaching

This method involves the extraction of silica nanoparticles from silica-rich precursors by use of sodium hydroxide at low temperatures. Mourhly *et al.*, (2019) demonstrated that it is feasible to isolate cost-effective silica nanoparticles from pumice volcanic rock using an alkaline extraction protocol. This method yielded 94 % pure amorphous silica nanoparticles with a high specific surface area ($422 \text{ m}^2\text{g}^{-1}$) and a mean pore diameter of 5.5 nm that was used as a support material for catalysis (Mourhly *et al.*, 2019). Silica-rich material is refluxed with 3 M NaOH at $100 \text{ }^\circ\text{C}$ for at least 4 hours while stirring to dissolve the silicate and form a Na_2SiO_3 solution as described in Equation 2.8 (Zulfiqar *et al.*, 2016).



The recovered Na_2SiO_3 is then acidified with drops of 5 M H_2SO_4 while stirring vigorously. Below pH 10, colloidal silica begins to precipitate and ends between pH 8 and 7. As shown in Equation 2.9, the process begins with the formation of weak and unstable silicic acid, which then condenses to form a network of silica gel as shown in Scheme 2.2.



Scheme 2.2: Condensation of Silicic Acid to form a Network of Silica Gel

The silica gel is then left to age at room temperature for 24 hours before being filtered and washed with deionized water to eliminate any remaining sulphate salts. Thereafter, its dried for 12 hours at $110 \text{ }^\circ\text{C}$ in an oven. The silica powder is further

refined by refluxing with 1 M HCl at 100 °C for 3 hours to remove any soluble minerals such as Fe, Al, Ca, and Mg. The suspension is then filtered, washed, and dried for 12 hours in an oven at 110 °C. Finally, its calcined in a muffle furnace at 550 °C for 2 hours, to yield a very fine white silica nanoparticles powder.

2.7 Sorption Isotherms Models

These are mathematical expressions applicable at constant temperature and are used in the analysis of adsorption data. There are several models such as Redlich-Peterson, Langmuir, Freundlich, Sips, Temkin, and Henry's isotherms. However, Langmuir and Freundlich's models are the simplest and most commonly used as they provide information on the maximum adsorption capacity of the adsorbent and how the solute interacts with the adsorbent during adsorption (Kalam *et al.*, 2021).

2.7.1 Freundlich Model

This model is used for a heterogeneous system based on the assumption that sorption takes place in several sites and as the number of adsorbates increases, the surface binding energy decreases exponentially which implies a multilayer formation. The model is expressed in Equations 2.10 and 2.11 (Nabbou *et al.*, 2019).

$$q_e = K_F C_e^{1/n} \text{ (Non - linear) } \dots\dots\dots 2.10$$

$$\text{Log } q_e = \text{Log } K_F + \frac{1}{n} \text{Log } C_e \text{ (Linear form) } \dots\dots\dots 2.11$$

Where;

C_e (mg/L) = adsorbate concentration at equilibrium.

q_e (mg/g) = amount of adsorbate adsorbed per unit mass of adsorbent.

K_F (mg/g) = constant (Freundlich coefficient) signifying the sorption capacity of the sorbent.

$1/n$ (unitless) = constant, signifying surface heterogeneity or adsorption intensity with its value ranging from 0.1 to 1 (Sadegh *et al.*, 2017). Adsorption is deemed favorable when $0 < 1/n < 0$, unfavorable when $1/n > 1$ and irreversible when $1/n = 1$ (Kalam *et al.*, 2021).

2.7.2 Langmuir Model

This model supposes that adsorbate species form a monolayer coverage on a homogeneous adsorbent surface with insignificant interactions of adsorbed species and that after a monolayer of adsorbate is formed the adsorbent is fully saturated. The Langmuir model is expressed using Equations 2.12 and 2.13 (Kofa *et al.*, 2017).

$$q_e = \frac{q_{max} K_L C_e}{1 + K_L C_e} \text{ (Non - linear).....2.12}$$

$$\frac{C_e}{q_e} = \frac{C_e}{q_{max}} + \frac{1}{K_L \times q_{max}} \text{ (Linear form).....2.13}$$

Where;

q_e (mg/g) = amount of adsorbate (fluoride) adsorbed per unit mass of adsorbent.

C_e (mg/L) = adsorbate equilibrium concentration.

q_{\max} (mg/g) = maximum monolayer adsorption capacity.

K_L = Langmuir constant depicting adsorbent affinity towards the adsorbate.

The suitability of the Langmuir model to fit the experimental data is evaluated by the use of separation factor (R_L) expressed by Equation 2.14:

$$R_L = \frac{1}{1 + K_L C_0} \dots \dots \dots 2.14$$

The value of R_L indicates whether the isotherm is favorable ($0 < R_L < 1$), unfavorable ($R_L > 1$), linear ($R_L = 1$), or irreversible ($R_L = 0$) (Akafu *et al.*, 2019).

2.8 Kinetic Models

Kinetic studies are used in determining the mechanisms and rates of sorption processes. A good adsorbent should have a fast rate of adsorption as well as a high adsorption capacity. Pseudo-first-order and pseudo-second-order models are the most commonly utilized models (Agarwal *et al.*, 2016).

2.8.1 Pseudo-First-Order Model

Pseudo-first-order is suitable for a simple sorption process where saturation occurs faster between 20-30 minutes. The expression for this model is illustrated in Equation 2.15 (Kariuki *et al.*, 2017).

$$\frac{dq_t}{dt} = K_1 (q_\infty - q_t) \dots \dots \dots 2.15$$

Integrating Equation 2.15 and linearizing we obtain Equations 2.16 or 2.17 (Pillai *et al.*, 2019).

$$\log (q_\infty - q_t) = \log q_\infty - \frac{K_1}{2.303} t \dots \dots \dots 2.16$$

$$\ln(q_e - q_t) = \ln q_e - K_1 t \dots\dots\dots 2.17$$

Where; q_t and q_e = amounts of adsorbate (mg/g) at time t , and equilibrium respectively. K_1 (Min⁻¹) = rate constant. A plot of $\log(q_e - q_t)$ versus time (t) gives a linear relationship. The values for q_e and K_1 are obtained from the intercept and slope respectively (Lin *et al.*, 2016).

2.8.2 Pseudo-Second-Order Model

The pseudo-second-order kinetic model assumes that chemisorption is the rate-controlling step in the sorption process. Equation 2.18 is the expression for this model (Kebede *et al.*, 2016).

$$\frac{dq_t}{dt} = K_2 (q_e - q_t)^2 \dots\dots\dots 2.18$$

Integrating Equation 2.18 and linearizing it we obtain Equation 2.19 (Pillai *et al.*, 2020).

$$\frac{t}{q_t} = \frac{1}{K_2 q_e^2} + \frac{1}{q_e} t \dots\dots\dots 2.19$$

Where;
 q_t and q_e = amounts of adsorbate (mg/g) at a time (t) and equilibrium respectively.

K_2 (g mg⁻¹ min⁻¹) = rate constant (Zhang *et al.*, 2017). A Plot of $\frac{t}{q_t}$ versus time (t)

gives a linear relationship. The amount of adsorbate adsorbed at equilibrium (q_e) and the rate constant (K_2) is determined from the slope and intercept, respectively (Kariuki *et al.*, 2017).

2.9 Techniques

2.9.1 Ion-Selective Potentiometry

Several analytical techniques can be used to determine the concentration of fluoride in water samples. Fluoride can be determined using Ion-chromatography, UV-Vis spectroscopy, or potentiometry using an Ion-selective electrode (ISE). However, ISE is mostly preferred since it is non-destructive, fast, and can analyze ions at trace levels as well as colored and viscous samples directly (Glu *et al.*, 2004). ISE has shortcomings such as deviation from Nernst's Equation due to changes in temperature, potential, and ion activity. However, these limitations can be eliminated quickly and readily. For instance, a shift in potential is solved by re-standardization, while a total ionic strength adjustment buffer (TISAB) is used to fix ion strength (Bratovcic & Catic, 2009). ISE is an electrochemical sensor that translates the activity of a specific ion in solution into an electrical potential. It has a selective membrane, a reference electrode, and a voltmeter. Potential difference is created by the movement of ions from high to low concentration through selective binding of ions with specific sites of the membrane. The potential is measured with respect to a reference standard electrode. The potential difference is directly proportional to the concentration of the selected ion present. A standard calibration curve is obtained by plotting electrode potential versus standard concentrations (Bratovčić & Čatić, 2009).

2.9.2 Characterization Techniques

Silica-based sorbent materials have been characterized by the use of techniques such as Scanning electron microscopy (SEM), X-ray diffraction (XRD), X-ray fluorescence (XRF), and Fourier transform infrared (FTIR) spectroscopy.

2.9.2.1 X-Ray Diffraction Spectroscopy

X-ray diffraction spectroscopy is a rapid nondestructive analytical technique used to determine the crystallographic structure of a material. In this technique, a material is irradiated with an incident X-ray then the scattering angles and intensities of the X-rays that leave the material are measured. The material is identified by its diffraction

patterns, which occur at specific angles (2θ) with respect to lattice spacing and are governed by Bragg's Law (Equation 2.20):

$$n\lambda = 2d\sin\theta \dots\dots\dots 2.20$$

Where n is an integer representing the order of reflection, λ is the wavelength of incident X-ray radiation, d is the interplanar spacing of the crystal and θ is the angle of incident radiation (Mourhly *et al.*, 2019). In previous studies, silica nanoparticles extracted from silica-rich precursors such as rice husks, sugarcane bagasse, and pumice rock were all of the amorphous phases, with a distinct single broad peak from 2θ of 15° to 30° and centered at 2θ of 22° (Rovani *et al.*, 2018).

2.9.2.2 Fourier Transform Infrared Spectroscopy

Fourier Transform Infrared (FTIR) spectroscopy is a vital and widely used technique for elucidating structure and identifying compounds. The functional groups present in a sample are identified using FTIR analysis; each functional group absorbs infrared radiation at specific frequencies (Rovani *et al.*, 2018). According to previous research, the broad peak observed on silica nanoparticles between 3000 and 3700 cm^{-1} and centered at 3352 cm^{-1} is due to the stretching vibration of the O-H bond from the silanol group, Si-OH (Imoisili *et al.*, 2020). A strong band at 1048 cm^{-1} corresponds to asymmetric stretching of the Si-O bond, whereas bands at 454 and 789 cm^{-1} relate to bending and symmetric stretching vibrations of the Si-O bond in the siloxane group, respectively (Yadav & Bhattacharyya, 2020).

2.9.2.3 X-Ray Fluorescence Spectroscopy

X-ray fluorescence (XRF) is a non-destructive, reliable, and rapid elemental analytical technique that measures the secondary X-ray (fluorescent) emitted by a sample when excited by a primary X-ray source. When excited, each element in the sample emits a unique X-ray with a characteristic wavelength and intensity ("fingerprint") that is proportional to the concentration of that element present. As a result, this method is used for both qualitative and quantitative analysis (Mohseni-Bandpei *et al.*, 2020). Previously, this technique was used to determine the chemical composition of pumice rock, and the results revealed that SiO_2 was the most

abundant mineral, accounting for 61.6 % (Soleimani *et al.*, 2019) and 63.4 % (Mohseni-Bandpei *et al.*, 2020).

2.9.2.4 Scanning Electron Microscopy

Scanning electron microscopy (SEM) is a critical technique used to obtain a detailed, high-quality, and spatially resolved image of a particle. In SEM, a sample is exposed to a high-energy electron beam that provides information about the topography, morphology, and crystallography of a material. Hence, SEM is a vital technique for the characterization of materials. Crystallography implies the arrangement of atoms in materials, morphology indicates the material's shape and size, whereas topography indicates the surface texture, smoothness, or roughness (Akhtar *et al.*, 2018).

CHAPTER THREE

MATERIALS AND METHODS

3.1 Study Area

Pumice rock and borehole water samples used in the study were collected from Paka volcano in Baringo County, Kenya ($36^{\circ} 10' 59''$ E and $0^{\circ} 55' 14''$ N) (Figure 3.1).

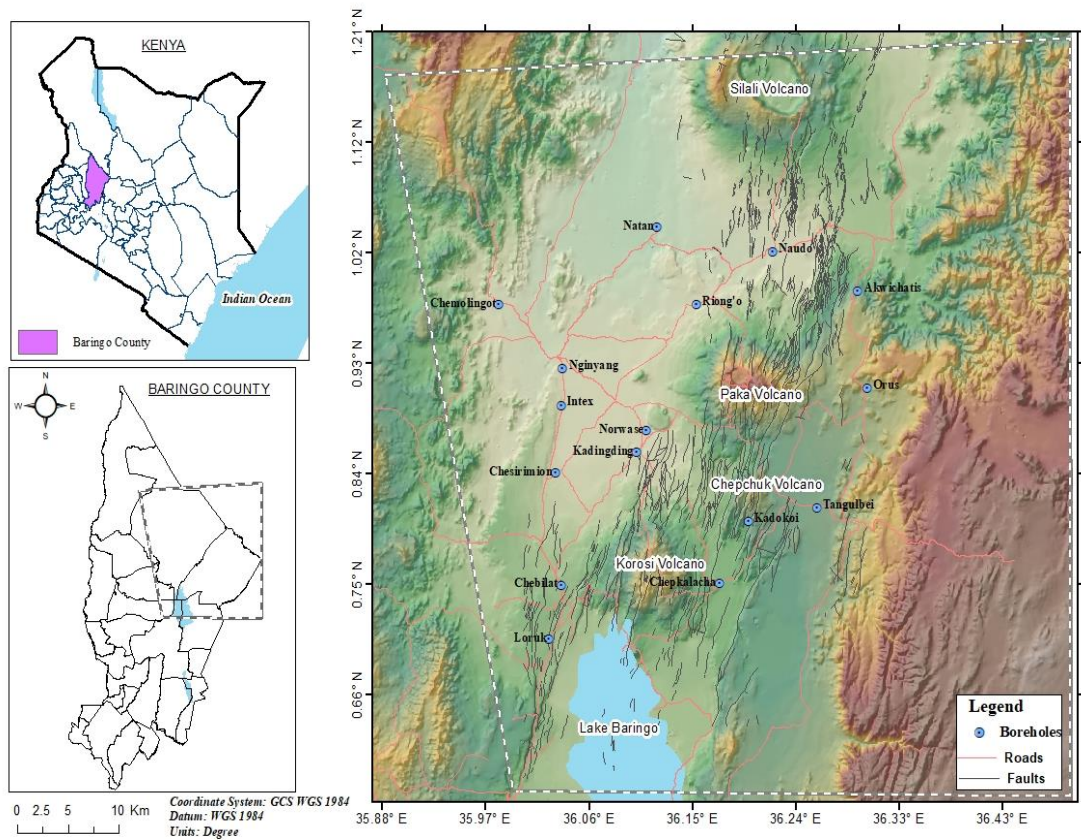


Figure 3.1: Location of Paka Volcano and Boreholes in Tiaty, Baringo in Kenya.

3.2 Samples Collection

With the assistance of a geologist in the field, approximately 5 kg of pumice rock was collected randomly in a clean well-label polythene sampling bag. Grab water samples were also randomly collected from boreholes in the study area (Figure 3.1)

in clean 1 L polyethylene bottles that were pretreated with dilute nitric acid and rinsed thoroughly with deionized water.

Samples for cations analysis were acidified with 1 mL concentrated HNO₃. Zinc acetate (2.5 % w/v) was added to samples for SO₄²⁻ analysis to avoid oxidation of sulphides to sulphate. No treatment was done to the samples to be analyzed for fluoride, chlorides, hardness, alkalinity, and bicarbonate levels. The samples were then transported within 24 hours to the Jomo Kenyatta University of Agriculture and Technology chemistry laboratory for analysis using the standard protocol defined by the American Public Health Association (APHA, 2022).

3.3 Instrumentation

The following instruments were used in this study: Hanna HI-935002 thermocouple thermometer (Woonsocket, United States), Jenway 430 pH/Conductivity meter (London, United Kingdom), Corning 400 flame photometer (Cambridge, United Kingdom), Elit 9801 ion meter (London, United Kingdom), Shimadzu AA-7000 spectrophotometer (Kyoto, Japan), Shimadzu UV-1800 spectrophotometer (Kyoto, Japan), Mettler-Toledo Titroline-7800 auto titrator (Columbus, United States), Rigaku ZSX Primus II X-ray fluorescence spectrophotometer (Tokyo, Japan), Rigaku MiniFlex II X-ray diffractometer (Tokyo, Japan), Shimadzu IRAffinity-1S Fourier Transform Infrared spectrophotometer (Kyoto, Japan) and JCM-7000-NeoScope Benchtop scanning electron microscope (Tokyo, Japan).

3.4 Chemicals and Reagents

The following analytical grade chemicals and reagents were used in this study: HNO₃ (69 %), HCl (35 %), H₂SO₄ (98 %), NaOH (99 %), KCl (99.8 %), NaCl (99.9 %), ethylenediaminetetraacetic acid (99 %), Eriochrome Black (98 %), ammonium buffer (99 %), pH buffers (99.9 %), phenolphthalein (99 %), methyl orange (99 %), ethyl alcohol (99.9 %), K₂CrO₄ (99 %), AgNO₃ (99.9 %), NaF (98 %), Na₂SO₄ (99.9 %), BaCl (95 %), La₂O₃ (99.9 %), CaCO₃ (96 %) and MgO (97 %) purchased from Sigma-Aldrich through Kobian Scientific Limited in Kenya and used without further

purification. Unless otherwise stated, deionized water was used throughout the analysis.

3.5 Determination of Physico-Chemical Water Quality Parameters

The physico-chemical water quality parameters were determined using the standard protocols as outlined by the American Public Health Association (APHA, 2022). In the field, a Hanna HI-935002 thermocouple thermometer (Woonsocket, United States) was used to measure water temperature, while a Jenway 430 pH/Conductivity meter (London, United Kingdom) was used to measure pH, electrical conductivity (EC) and total dissolved solid (TDS). Total hardness was determined using a complexometric titration with 0.01 M ethylenediaminetetraacetic acid (EDTA) and Eriochrome Black T (EBT) indicator; at the end-point, the solution changed from wine red to blue. Total alkalinity and bicarbonates were determined using titrimetry with 0.1 N HCl using phenolphthalein and methyl-orange indicators.

The concentrations of potassium and sodium were determined using a Corning 400 flame photometer (Cambridge, United Kingdom) with working standards of 5, 10, 20, 40, 80, and 100 mg/L and 5, 8, 10, 20, 30, and 40 mg/L, respectively. Calcium and magnesium were determined using a Shimadzu AA-7000 spectrophotometer (Kyoto, Japan) with working standards of 1, 2, 4, 6, 8, and 10 mg/L and 0.5, 1, 1.5, 2, and 2.5 mg/L, respectively. In addition, 1 mL of 50 mg/L La_2O_3 solution (releasing agent) was mixed with 10 mL of each standard, sample, and blank. Chloride levels were determined using argentometric titration with 0.1 N AgNO_3 and 5 % K_2CrO_4 indicator; at the end-point, the solution changed from yellow to red-brown. Sulphate levels were assessed using turbidimetry with a Shimadzu UV-1800 spectrophotometer (Kyoto, Japan). The working standards were 2.5, 5, 10, 15, and 30 mg/L, and 3 mL of sulphate conditioning reagent was added to 5 mL of each standard, samples, and blank in 100 mL volumetric flasks, followed by a spatula full of BaCl_2 , and the absorbances were measured at 425 nm after shaking. Fluoride levels were determined using potentiometry with an Elit 9801 ion meter (London, United Kingdom) equipped with a fluoride ion selective electrode (ISE) and a reference electrode. The working standards were 2, 4, 6, 8, 10, and 20 mg/L, and 5

mL of TISAB was mixed and shaken thoroughly with 5 mL of each standard, sample, and blank prior to recording the potential developed.

3.6 Extraction, Modification, and Characterization of Silica Particles

3.6.1 Pretreatment of Pumice Rock

Pumice rock was washed several times with deionized water to remove any impurities until the pH was neutral, dried, and then pulverized using a Retsch PM 400 Model Planetary ball mill pulverizer (New Hampshire, United States). The ground powder was then passed through a 180 μm sieve to obtain homogeneous particle sizes. It was finally activated using a Sentrotech STT-1200C-3.5-12 muffle furnace (Strongsville, United States) for 3 hours at 550 $^{\circ}\text{C}$ followed by the isolation of silica particles using the method proposed by Mourhly *et al.*, (2019).

3.6.2 Extraction of Silica Particles (SPs) from Pumice Rock

Silica particles were extracted in triplicate using a low-temperature alkaline leaching protocol described by Mourhly *et al.*, (2019). 10 g of ground pumice was refluxed with 300 mL of 3 M NaOH at 100 $^{\circ}\text{C}$ for 4 hours while stirring at 300 rpm to dissolve the silicate and form a Na_2SiO_3 solution (Zulfiqar *et al.*, 2016). To recover Na_2SiO_3 , the slurry was filtered with ashless filter paper (Whatman No 41). The filtrate was then acidified by adding a few drops of 5 M H_2SO_4 to pH 7 while vigorously stirring to form silica gel (Imoisili *et al.*, 2020). The silica gel was allowed to age for 12 hours before the filtration and washing step. The gel was then dried for 12 hours at 110 $^{\circ}\text{C}$ followed by refluxing with 1 M HCl for 3 hours at 100 $^{\circ}\text{C}$ to remove any soluble minerals such as Fe, Al, Ca, and Mg. The suspension was filtered, washed, and dried for 12 hours at 110 $^{\circ}\text{C}$. The final product was activated for 3 hours in a Sentrotech STT-1200C-3.5-12 muffle furnace (Strongsville, United States) at 550 $^{\circ}\text{C}$ to yield fine white silica particles (SPs) powder.

The amount of silica recovered from pumice rock was calculated using Equation 3.1 (Mourhly *et al.*, 2019).

$$\text{SPs yield (\%)} = \left(\frac{\text{Weight of extracted SPs (g)}}{\text{Weight of silica in pumice rock (g)}} \right) \times 100 \dots \dots \dots 3.1$$

The weight of silica in pumice rock is the product of the weight of pumice rock used in the extraction and the percent SiO₂ obtained from XRF analysis.

3.6.2.1 Modification of SPs with Iron

The silica particles were modified with iron according to the method proposed by El-Moselhy *et al.*, 2017. In a 50 mL solution containing 1 g of Fe(NO₃)₃·9H₂O, 10 g of silica particles were dissolved. The pH of the solution was adjusted to 7 with 0.5 M NaOH and then stirred at room temperature for 1 hour. The mixture was centrifuged, and the resulting particles were washed and dried for 12 hours at 105 °C. Finally, the Fe-modified silica particles (FMSPs) were activated in a muffle furnace for 6 hours at 500 °C and preserved in a clean high-density polyethylene (HDPE) container.

3.6.3 Characterization

The bulk chemical composition of pumice rock, silica particles (SPs), and Fe-modified silica particles (FMSPs) was determined using Rigaku ZSX Primus II X-ray fluorescence spectrophotometer (Tokyo, Japan). For phase identification, a Rigaku MiniFlex II X-ray diffractometer (Tokyo, Japan) with copper radiation (CuKα = 1.5418 Å) operating at 15 mA and 30 kV was used to record diffractograms between 2θ of 3° and 50°, with a step size of 0.02 at 2 seconds per step. The functional groups were identified using a Shimadzu IRAffinity-1S Fourier transform Infrared spectrophotometer (Kyoto, Japan) in attenuated total reflectance mode, with spectra recorded between 4000 and 400 cm⁻¹ with a resolution of 4 cm⁻¹. The morphology of the silica particles was examined using a JCM-7000- NeoScope Benchtop scanning electron microscope (Tokyo, Japan).

3.7 Batch Adsorption Studies

Batch experiments were conducted at room temperature to determine the optimal pH, sorbent dose, contact time, and initial fluoride concentration for fluoride removal using FMSPs as described in Sections 3.7.1 to 3.7.4. Equations 3.2 and 3.3 were used to calculate the amount of fluoride adsorbed at equilibrium (q_e) and the percentage of fluoride removed (Gogoi *et al.*, 2018).

$$q_e = \frac{V(C_o - C_e)}{m} \dots\dots\dots 3.2$$

$$\% \text{ Sorption} = \frac{C_o - C_e}{C_o} \times 100 \dots\dots\dots 3.3$$

Where;

m (g) = sorbent mass.

V (L) = volume of the solution.

q_e (mg/g) = amount of fluoride adsorbed at equilibrium.

C_o and C_e (mg/L) = initial and equilibrium fluoride concentrations, respectively

(Borgohain *et al.*, 2020).

3.7.1 Optimization of pH

The effect of pH on fluoride removal was investigated using 1.5 g of FMSPs and 250 mL of a 20 mg/L fluoride solution. The pH was varied from 2, 3, 4, 5, 6, 7, 8, 9 to 10 using 0.5 M $\text{CH}_3\text{COOH}/\text{CH}_3\text{COONa}$ and 0.5 M $\text{NH}_4\text{OH}/\text{NH}_4\text{Cl}$ buffers. The solutions were stirred at room temperature for 90 minutes before being filtered with

Whatman No. 42 filter paper. The residual fluoride concentration in the filtrate was then determined using an ion-selective electrode (ISE).

3.7.2 Optimization of Sorbent Dose

The effect of sorbent dose on defluoridation was evaluated by equilibrating various sorbent doses of 0.2, 0.4, 0.6, 0.8, 1.0, 1.5, 2.0, and 2.5 g with 250 mL of a 20 mg/L fluoride solution at the optimum pH of 6. The solutions were stirred at room temperature for 90 minutes before being filtered with Whatman No. 42 filter paper. The residual fluoride concentration in the filtrate was then determined using an ISE.

3.7.3 Optimization of Contact Time

The adsorption capacity of FMSPs as a function of time was studied using 250 mL of a 20 mg/L initial fluoride solution at optimal pH (6) and sorbent dose (1 g) by varying contact time from 5, 10, 15, 20, 25, 30, 35, 40, 45, 50, 60 to 90 minutes. After stirring the solutions for a predetermined time at room temperature, they were left to settle for 2 minutes before filtration with Whatman No. 42 filter paper. The concentration of residual fluoride in the filtrates was then determined using an ISE.

3.7.4 Optimization of Initial Fluoride Concentration

The effect of initial fluoride concentration on defluoridation was studied using optimal pH (6), dose (1 g), and contact time (45 minutes), and the initial fluoride concentration was varied from 2.5, 5, 10, 15, 20, 30, 40, 50 to 60 mg/L. After stirring the solutions for 45 minutes at room temperature, they were left to settle for 2 minutes followed by filtration with Whatman No. 42 filter paper and analysis of residual fluoride.

3.7.5 Adsorption Isotherms and Kinetic Models

The adsorption data was fitted in both the Langmuir and Freundlich adsorption models (Ismail *et al.*, 2014). The rate and mechanism of defluoridation were evaluated using pseudo-first-order and pseudo-second-order kinetics models (Sadegh *et al.*, 2017).

3.8 Removal of Fluoride from Real Water Samples

Borehole water samples collected from Tiaty in Baringo County, Kenya, were utilized to evaluate the efficiency of Fe-modified silica particles (FMSPs) in defluoridation. Apart from filtration with Whatman No. 42 filter paper, the samples were used without any other treatments. The initial fluoride levels were determined, and then defluoridation was performed using the optimal sorbent dose (1 g) and contact time (45 minutes). The residual fluoride levels were then determined.

3.9 Regeneration Studies

A batch desorption experiment was done according to Rafique and colleagues with slight modifications to evaluate the ability of adsorbents to be regenerated and recycled (Rafique *et al.*, 2013). Five consecutive cycles of adsorption-desorption experiments were done using 0.1 M NaOH as a desorbing agent. The spent sorbent was soaked in NaOH for 2 hours, washed with deionized water until the washed water pH was 7 then dried in an oven at 90 °C for 4 hours. A fluoride solution of 20 mg/L initial concentration was used with optimum sorbent dose (1 g) and contact time (45 minutes).

CHAPTER FOUR

RESULTS AND DISCUSSION

4.1 Physico-Chemical Water Quality Parameters

The borehole temperature ranged from 27.4 - 40.7 °C (Table 4.1), whereas ambient is the ideal temperature for drinking, elevated temperatures can influence the odor, color, and taste of water (Chebet *et al.*, 2020). The elevated temperature of up to 40.7°C for Riong'o borehole could be attributed to being within or close to the Paka geothermal system, which can heat up the groundwater (Figure 3.1). As water seeps underground and comes into contact with hot rocks or magma chambers, it can become heated to high temperatures. The pH ranged between 6.79 - 8.70 (Table 4.1) with a mean of 7.94 ± 0.60 . The slightly alkaline water is attributed to volcanic rocks in the aquifers that are rich in minerals such as sodium, potassium, magnesium, and calcium. In addition, the high temperature associated with volcanic activities can also increase groundwater alkalinity by promoting the leaching of aquifer minerals. The allowable pH limit for drinking water is 6.5 - 8.5 (WHO, 2017); all boreholes except Riong'o were within this range. The apparent effect of high pH in drinking water is a soda-like taste and a slick feeling.

The EC values ranged from 402.89 - 4212.99 μScm^{-1} . Except for the Riong'o borehole, EC values in this survey were under the WHO criterion of 2500 μScm^{-1} (Table 4.1). High EC implies an enrichment of soluble ionic species in the water. The TDS values ranged from 201.24 - 2111.77 mg/L (Table 4.1) and the recommended limit is 500 - 1500 mg/L (WHO, 2017), hence the Riong'o borehole surpassed this limit. According to Boadi *et al.*, (2020) when the temperature of the water rises, so do the EC and TDS. As a result, the higher EC and TDS in the Riong'o borehole could be attributable to aquifer mineral dissolution aided by high temperatures. Drinking water with high TDS can cause gastrointestinal irritation, formation of kidney stones, and heart attack (Udhayakumar *et al.*, 2016). Elevated TDS also influences the taste, hardness, and corrosive properties of water (Arulnangai *et al.*, 2019).

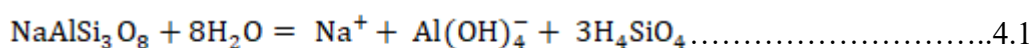
Table 4.1: Results for Onsite Analysis, Alkalinity, and Hardness (n = 3)

| Site Name | Temp. (°C) | pH | EC (µS/cm) | Concentration in mg/L | | |
|-----------|-------------|-------------|----------------|-----------------------|------------------|----------------|
| | | | | TDS | Total Alkalinity | Total Hardness |
| Intex | 35.7 ± 0.19 | 8.20 ± 0.01 | 564 ± 1.28 | 282.59 ± 0.85 | 100.23 ± 0.71 | 56.17 ± 0.58 |
| Riong'o | 40.7 ± 0.30 | 8.70 ± 0.01 | 4212.99 ± 2.82 | 2111.77 ± 1.41 | 1142.78 ± 1.32 | 519.72 ± 1.15 |
| Kadokoi | 31.5 ± 0.25 | 8.12 ± 0.01 | 677.62 ± 1.82 | 340.34 ± 0.91 | 200.12 ± 0.58 | 102.65 ± 0.76 |
| Nginyang | 33.1 ± 0.37 | 6.79 ± 0.00 | 402.89 ± 1.47 | 201.24 ± 0.74 | 96.86 ± 1.00 | 36.82 ± 0.40 |
| Tangulbei | 36.8 ± 0.40 | 8.01 ± 0.00 | 866.94 ± 1.92 | 433.04 ± 0.96 | 320.17 ± 1.50 | 72.35 ± 0.62 |
| Naudo | 37.3 ± 0.27 | 8.30 ± 0.01 | 1657.87 ± 2.24 | 917.11 ± 1.12 | 464.91 ± 1.31 | 104.57 ± 0.82 |
| Orus | 27.4 ± 0.25 | 7.36 ± 0.00 | 440.71 ± 1.38 | 244.33 ± 0.69 | 136.13 ± 1.39 | 78.15 ± 1.04 |
| Akuchatis | 33.1 ± 0.32 | 8.05 ± 0.01 | 1252.77 ± 1.43 | 623.27 ± 0.72 | 416.87 ± 0.89 | 190.83 ± 0.75 |

Hard water is defined as water that does not easily lather with soap and is primarily caused by Ca^{2+} , Mg^{2+} , CO_3^{2-} , SO_4^{2-} , Cl^- and HCO_3^- (Prasanth *et al.*, 2012). For this study, total hardness was in the range 36.82 - 519.72 mg/L (Table 4.1), except for Riong'o borehole, which measured 519.72 ± 1.15 mg/L, all of which were within or below the WHO standard of 100 - 500 mg/L (WHO, 2017). Water hardness can elevate the boiling point of water and cause scaling in pipes, heaters, and boilers (Bamigboye *et al.*, 2020). Drinking hard water can lead to renal and cardiac disorders in humans (Udhayakumar *et al.*, 2016).

Alkalinity is the ability of water to neutralize acid and is an estimation of hydroxides, carbonates, and bicarbonates levels in water (Karthika *et al.*, 2018). For this survey, it ranged from 96.86 - 1142.78 mg/L (Table 4.1), with Riong'o, Tangelbei, Naudo, and Akwichatis boreholes surpassing the WHO guideline of 200 mg/L (WHO, 2017). The elevated alkalinity levels can be attributed to the presence of dissolved minerals such as bicarbonates, carbonates, and hydroxides of calcium, magnesium, potassium, and sodium leached from alkaline volcanic rock in the aquifers.

The levels of major ions in borehole water are shown in Table 4.2 while their corresponding calibration curves are presented in Appendices I - VI. The most prevalent cation was sodium, its levels ranged from 46.81 - 856.37 mg/L (Table 4.2), and it exceeded the WHO acceptable limit of 200 mg/L (WHO, 2017) in the Naudo and Riong'o boreholes. This may be due to input from circulating geothermal fluids and chemical weathering of albite (Equation 4.1), a sodium-rich mineral invariably found in volcanic rocks (Rusiniak *et al.*, 2021).



High blood pressure, arteriosclerosis, hyperosmolarity, and edema can all be caused by an excess of sodium in drinking water (Prasanth *et al.*, 2012).

Table 4.2: Concentrations of Major Ions (n = 3)

| Site Name | mg/L | | | | | | | |
|-----------|-----------------|----------------|------------------|------------------|-----------------|-------------------------------|-------------------------------|----------------|
| | Na ⁺ | K ⁺ | Ca ²⁺ | Mg ²⁺ | Cl ⁻ | SO ₄ ²⁻ | HCO ₃ ⁻ | F ⁻ |
| Intex | 114.51 ± 2.06 | 12.65 ± 1.18 | 2.43 ± 0.02 | 1.38 ± 0.24 | 19.85 ± 1.11 | 22.59 ± 0.46 | 233.0 ± 1.86 | 4.57 ± 0.06 |
| Riong'o | 856.37 ± 2.51 | 26.49 ± 1.89 | 1.73 ± 0.01 | 2.22 ± 1.33 | 288.02 ± 1.29 | 95.31 ± 0.89 | 1453.2 ± 2.43 | 16.47 ± 0.29 |
| Kadokoi | 117.76 ± 1.49 | 10.64 ± 1.17 | 20.12 ± 0.05 | 13.68 ± 0.04 | 68.09 ± 0.74 | 37.93 ± 0.21 | 254.0 ± 1.23 | 2.46 ± 0.10 |
| Nginyang | 59.64 ± 1.36 | 10.12 ± 1.54 | 4.85 ± 0.01 | 3.05 ± 0.05 | 22.69 ± 0.98 | 15.62 ± 0.19 | 127.1 ± 0.98 | 1.35 ± 0.05 |
| Tangulbei | 163.47 ± 1.70 | 6.08 ± 1.01 | 17.33 ± 0.02 | 18.71 ± 0.21 | 65.45 ± 1.20 | 24.47 ± 0.30 | 390.4 ± 1.36 | 1.33 ± 0.02 |
| Naudo | 325.51 ± 2.63 | 19.42 ± 1.77 | 7.39 ± 0.01 | 7.81 ± 0.37 | 155.99 ± 1.45 | 22.77 ± 0.47 | 566.1 ± 2.67 | 5.39 ± 0.31 |
| Orus | 46.81 ± 1.07 | 8.41 ± 1.61 | 20.91 ± 0.01 | 10.01 ± 0.23 | 22.69 ± 1.63 | 16.42 ± 0.32 | 170.9 ± 0.97 | 0.88 ± 0.01 |
| Akuchatis | 188.76 ± 1.32 | 8.6 ± 1.36 | 30.84 ± 0.03 | 29.44 ± 0.16 | 96.43 ± 1.56 | 28.59 ± 0.45 | 507.5 ± 1.38 | 1.29 ± 0.04 |

The potassium concentration ranged from 6.08 - 26.49 mg/L (Table 4.2). Weathering of K-feldspar-bearing rocks and clay minerals from the volcanic aquifers may be the cause of potassium levels above the WHO limit of 12 mg/L in Naudo, Intex, and Riong'o (Ochieng *et al.*, 2012). Potassium is essential in the human body for functions such as water balance, blood pressure, nerve impulses, muscle contraction, digestion, and pH balance (Meride & Ayenew, 2016).

Calcium is required for bone and tooth development in the body; in this study, it ranged from 1.73 - 30.84 mg/L (Table 4.2), with no borehole exceeding the WHO limit of 200 mg/L (WHO, 2017).

The magnesium levels ranged from 1.38 - 29.41 mg/L (Table 4.2), with all boreholes falling within the WHO threshold of 150 mg/L (WHO, 2017). While magnesium is necessary for cardiovascular health, it may have a laxative effect on drinking water (Arulnagai *et al.*, 2019).

Chloride levels ranged from 19.85 - 288.02 mg/L (Table 4.2), with only Riong'o surpassing the WHO limit of 250 mg/L (WHO, 2017). The elevated chloride levels could be attributed to the leaching of chloride ions from volcanic rocks and minerals into the groundwater. In addition, Riong'o borehole is adjacent to the Paka geothermal system (Figure 3.1). Geothermal fluids usually contain high concentrations of chloride ions, which can mix with groundwater and increase the overall chloride levels. Drinking chloride-rich water has been linked to kidney and heart problems (Udhayakumar *et al.*, 2016).

The sulphate concentration ranged from 15.62 - 95.31 mg/L (Table 4.2), with no borehole exceeding the allowed peak of 400 ppm (WHO, 2017). Excess sulphate levels in drinking water can cause dehydration as well as diarrhea (Chebet *et al.*, 2020).

Bicarbonate was the most prevalent anion in the range of 127.1 - 1453.2 mg/L (Table 4.2). This trend is consistent with previous research on groundwater in

Kenya's Rift Valley and has been attributed to the conversion of the abundant magmatic CO_2 to HCO_3^- (Gevera & Mouri, 2018; Mwiathi *et al.*, 2022).

4.2 Fluoride Levels

Fluoride levels in the borehole water varied from 0.88 ± 0.11 to 16.4 ± 0.29 mg/L (Figure 4.1), with Intex, Riong'o, Kadokoi, and Naudo boreholes exceeding the WHO standard of 1.5 mg/L (WHO, 2017). Appendix VI shows the standard calibration curve for fluoride.

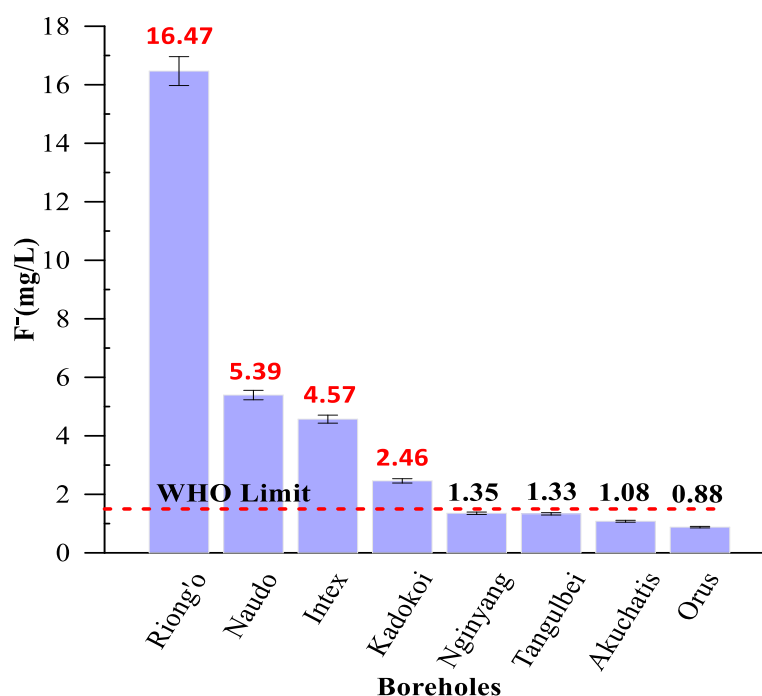


Figure 4.1: Fluoride Levels in Borehole Water

The study area is located around the Korosi, Chepchuk, Paka, and Silali quaternary volcanoes (Figure 3.1), which are part of the East African Rift Valley System. The groundwater occurs in fractured zones in volcanic rocks containing fluoride-bearing minerals such as sellaite (MgF_2), cryolite (Na_3AlF_6), fluorapatite ($\text{Ca}_5(\text{PO}_4)_3\text{F}$), fluorite (CaF_2), villiaumite (NaF) and topaz ($\text{Al}_2(\text{SiO}_4)\text{F}_2$) (Mutonga, 2014; Mwiathi *et al.*, 2022). Therefore, the high fluoride level in boreholes (Figure 4.1) is likely due to interactions between water and these fluoride-bearing minerals present in bedrocks

as well as hydrothermal input from fumaroles and circulating magmatic fluids in permeable faults which have a significant amount of fluoride.

4.2.1 Statistical Correlation Analysis

Spearman's correlation was used to assess the strength and direction of the relationship between fluoride and other physico-chemical parameters. Fluoride correlates strongly with pH ($R^2 = 0.993$) in groundwater with high fluoride levels (Figure 4.2), indicating that alkaline groundwater favors the solubility of fluoride-bearing minerals. This suggests that the pH of water is very important in determining fluoride concentration. Furthermore, the strong correlation between pH and fluoride suggests that fluoride may be leached under alkaline water conditions. This is owing to the similarity of charge and ionic radii for F^- (1.36 Å) and OH^- (1.40 Å) (Brahman *et al.*, 2013) thereby replacing each other at higher pH, resulting in fluoride enrichment in groundwater.

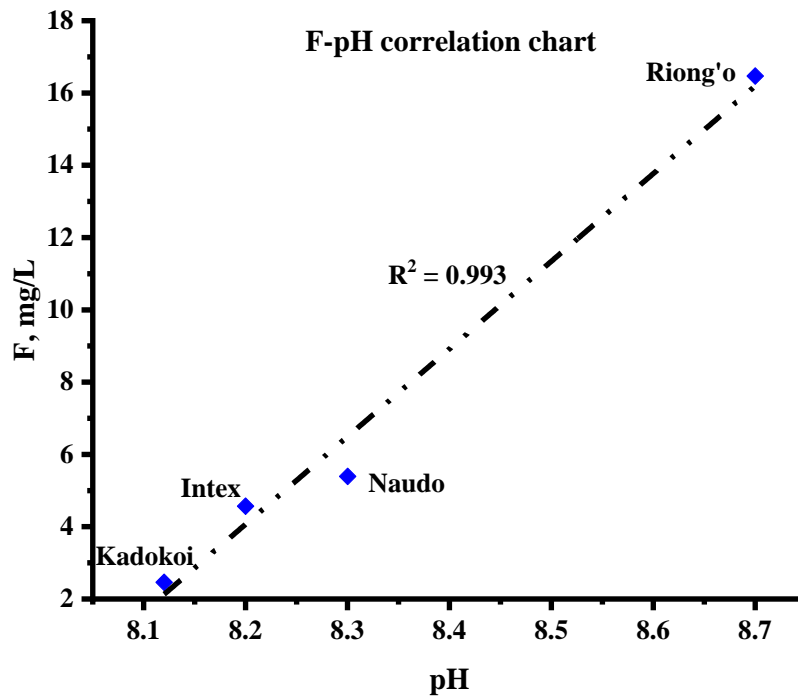


Figure 4.2: The Correlation between Fluoride and pH for Fluoride-Rich Boreholes

The correlation between fluoride and TDS is strong ($R^2 = 0.939$), as shown in Table 4.3. This indicates that an increase in TDS causes an increase in fluoride concentration in groundwater. TDS in groundwater is caused by salts of Cl^- , SO_4^{2-} , K^+ , HCO_3^- and Na^+ , which play an important role in achieving a favorable pH for the dissolution of fluoride-bearing minerals in the bedrock. Fluoride has a strong linear correlation with Cl^- , SO_4^{2-} , K^+ , HCO_3^- and Na^+ , whereas Mg^{2+} and Ca^{2+} have a weak and negative correlation with fluoride (Table 4.3).

Table 4.3: Statistical Correlation Matrix for Physico-Chemical Parameters

| | F ⁻ | TDS | HCO ₃ ⁻ | Cl ⁻ | SO ₄ ²⁻ | Na ⁺ | K ⁺ | Ca ²⁺ | Mg ²⁺ |
|-------------------------------|----------------|-------|-------------------------------|-----------------|-------------------------------|-----------------|----------------|------------------|------------------|
| F ⁻ | 1 | | | | | | | | |
| TDS | 0.939 | 1 | | | | | | | |
| HCO ₃ ⁻ | 0.923 | 0.993 | 1 | | | | | | |
| Cl ⁻ | 0.890 | 0.984 | 0.973 | 1 | | | | | |

| | | | | | | | | | |
|------------------------------------|--------|--------|--------|--------|--------|--------|--------|-------|---|
| SO₄²⁻ | 0.920 | 0.917 | 0.929 | 0.880 | 1 | | | | |
| Na⁺ | 0.959 | 0.996 | 0.991 | 0.973 | 0.933 | 1 | | | |
| K⁺ | 0.936 | 0.888 | 0.839 | 0.875 | 0.778 | 0.893 | 1 | | |
| Ca²⁺ | -0.598 | -0.364 | -0.310 | -0.294 | -0.312 | -0.418 | -0.637 | 1 | |
| Mg²⁺ | -0.491 | -0.213 | -0.143 | -0.129 | -0.223 | -0.263 | -0.542 | 0.919 | 1 |

The solubility product principle explains the negative correlation fluoride has with magnesium and calcium. According to this principle, an increase in fluoride levels will automatically cause a decrease in magnesium and/or calcium in water (Addison *et al.*, 2020).

4.3 Extraction, Modification, and Characterization of Silica Particles

4.3.1 Silica Yield

The results for the amount of silica particles extracted from pumice rock are shown in Table 4.4. An average of 5.30 ± 0.37 g silica particles (SPs) were recovered from 9.99 ± 0.01 g pumice rock, representing 86.43 ± 0.41 % yield. This implies that alkaline leaching of silica particles from pumice rock is feasible. The yield from this study was slightly less than to that obtained by Mourhly *et al.*, (2019).

Table 4.4: Recovery of Silica Particles from Pumice Rock (n = 3)

| Pumice rock | Weight (g) | | Extraction efficiency (%) |
|-----------------|---|-----------------------------------|---------------------------|
| | SiO ₂ in pumice rock from XRF analysis | SiO ₂ after extraction | |
| 9.99 ± 0.01 | 6.13 ± 0.18 | 5.30 ± 0.37 | 86.43 ± 0.41 |

4.3.2 Characterization

4.3.2.1 XRF Analysis

Table 4.5 shows the chemical components of pumice rock, silica particles (SPs), and Fe-modified silica particles (FMSPs) derived from XRF analysis. The main components are SiO_2 (61.41 ± 0.19 %), Al_2O_3 (12.07 ± 0.24 %) and Fe_2O_3 (11.06 ± 0.63 %). Similarly, in previous research, SiO_2 was reported to be the most abundant component of pumice rock, accounting for 61.6 % (Soleimani *et al.*, 2019) and 63.4 % (Mohseni-Bandpei *et al.*, 2020).

Table 4.5: Chemical Composition of Pumice Rock, SPs, and FMSPs

| Components | Composition (% w/w) | | |
|--------------------------------|---------------------|--------------|--------------|
| | Pumice rock | SPs | FMSPs |
| SiO ₂ | 61.41 ± 0.19 | 97.71 ± 0.19 | 93.67 ± 0.66 |
| Al ₂ O ₃ | 12.07 ± 0.24 | | |
| Fe ₂ O ₃ | 11.06 ± 0.63 | | 2.93 ± 0.02 |
| CaO | 1.11 ± 0.01 | | |
| MgO | 0.18 ± 0.07 | | |
| SO ₃ | 0.10 ± 0.01 | | |
| K ₂ O | 5.51 ± 0.13 | | |
| Na ₂ O | 6.36 ± 0.45 | | |
| P ₂ O ₅ | 0.08 ± 0.01 | | |
| MnO | 0.45 ± 0.01 | | |
| Loss on ignition | 1.67 ± 0.16 | 2.29 ± 0.21 | 3.4 ± 0.41 |

As indicated in Table 4.5, the retrieved SPs are largely comprised of SiO₂. The absence of other oxides previously present in raw pumice rock, along with the high silica content of 97.71 ± 0.19 %, implies that relatively pure SPs were extracted. SiO₂ and Fe₂O₃ contents in FMSPs were 93.67 ± 0.66 % and 2.93 ± 0.02 %, respectively. The reduction in SiO₂ from 97.71 ± 0.19 % (SPs) to 93.67 ± 0.66 % (FMSPs) with the addition of Fe₂O₃, which was not present in pure SPs, reveals that the iron coating of SPs was effective.

4.3.2.2 XRD Analysis

An X-ray diffractometer was used to identify the minerals present in pumice rock, SPs, and FMSPs. According to the diffractograms in Figure 4.3, pumice rock comprises crystalline phase minerals, primarily anorthoclase, feldspar, and quartz (Noori *et al.*, 2014).

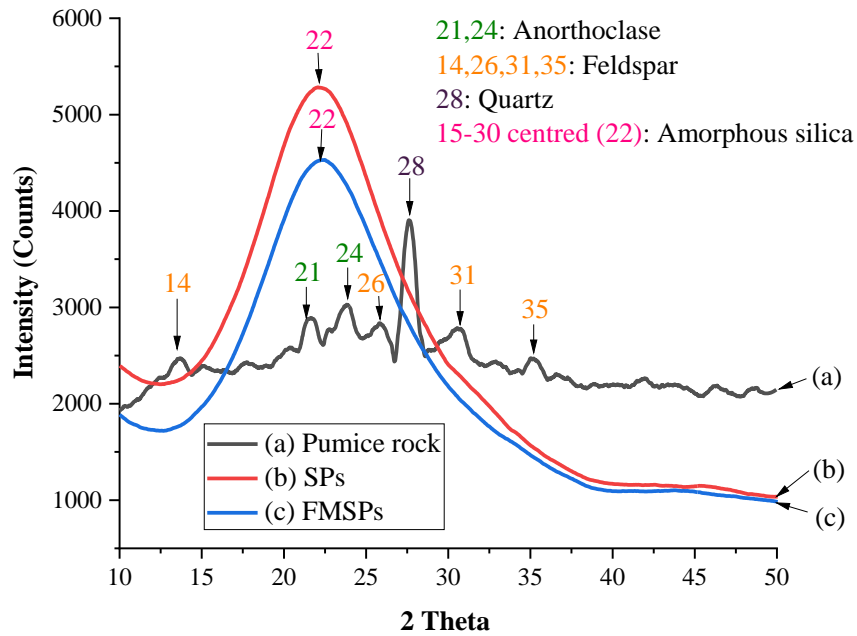


Figure 4.3: Diffractograms of (a) Pumice Rock, (b) SPs, and (c) FMSPs

The extracted silica particles exhibited a single broad peak from 2θ of 15° to 30° , centered at 2θ of 22° (Figure 4.3), which is a distinctive feature of amorphous silica (Rovani *et al.*, 2018). The absence of crystalline peaks previously observed in pumice rock confirms that the isolated SPs were predominantly amorphous (Zulfiqar *et al.*, 2016). The Fe-coated silica particles were likewise amorphous.

4.3.2.3 FTIR Spectrophotometry Analysis

The functional groups present in pumice rock, SPs, and FMSPs are depicted in Figure 4.4. The stretching vibration of the O-H bond from the silanol group (Si-OH) is responsible for the very weak vibrational band observed between $3000 - 3700 \text{ cm}^{-1}$ and centered at 3352 cm^{-1} (Imoisili *et al.*, 2020). This band was attributed to surface-adsorbed water on silica particles.

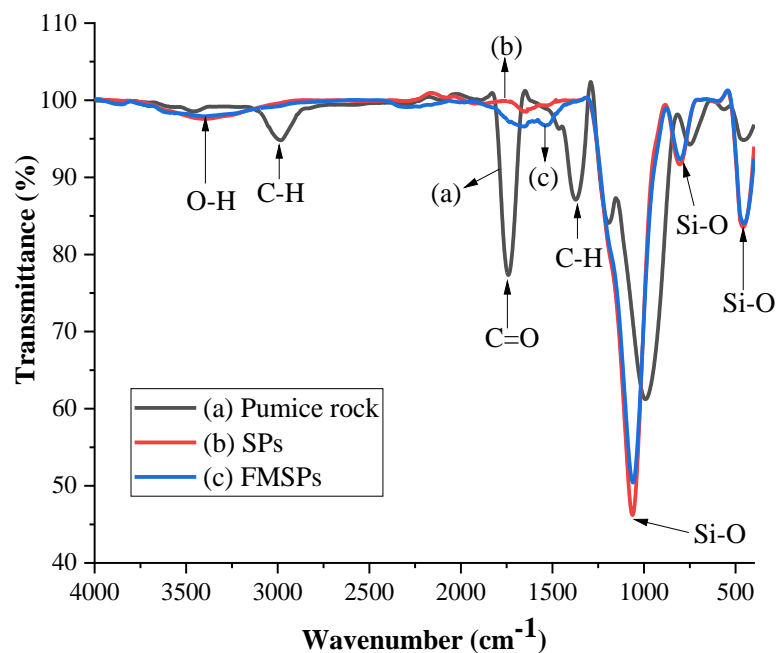


Figure 4.4: FTIR Spectra of Pumice Rock (a), SPs (b), and FMSPs (c)

A strong band at 1048 cm^{-1} (Figure 4.4) corresponds to asymmetric stretching of the Si-O bond, whereas bands at 454 and 789 cm^{-1} relate to bending and symmetric stretching vibrations of the Si-O bond in the siloxane group, respectively (Yadav & Bhattacharyya, 2020). Similar observations were made by Mourhly *et al.*, (2015) while extracting silica nanoparticles from pumice rock. The bands at 2985 , 1741 , and 1375 cm^{-1} on the pumice rock are attributed to the C-H stretch, C=O stretch, and C-H bend, respectively (Suneetha *et al.*, 2015). On the other hand, FMSPs had similar vibrational bands as those of SPs (Figure 4.4). However, there was a slight decrease in the intensity of the Si-O vibrational band at 1048 cm^{-1} attributed to the interaction of iron ions with the silica matrix. The interaction can cause changes in bond strength as well as the geometry of the Si-O bonds, resulting in a slight decrease in vibrational intensity. The absence of vibrational bands associated with iron-silica in the FTIR spectrum of FMSPs could be due to the low concentration of iron in the modified silica particles that could not be easily detectable due to their low intensity or overlap with other vibrational bands.

4.3.2.4 SEM Analysis

The SEM micrographs in Figure 4.5 demonstrate that the extracted silica particles were spherical and agglomerated together to form clusters. This denotes amorphous silica and is consistent with XRD data (Figure 4.3). A similar finding was made when silica particles were extracted from pumice rock (Mourhly *et al.*, 2019).

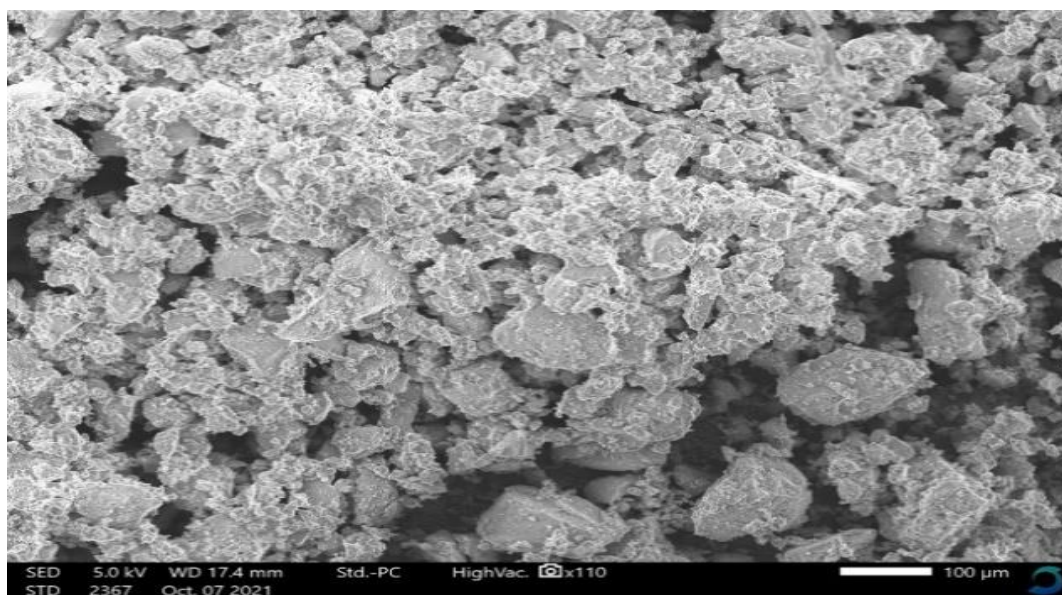


Figure 4.5: SEM Micrograph for Extracted Silica Particles

4.4 Adsorption Studies

Batch experiments were conducted at room temperature to determine the optimal pH, sorbent dose, contact time, and initial fluoride concentration for fluoride removal using FMSPs. Their corresponding raw data are presented in Appendices VII-X.

4.4.1 Effect of pH

The effect of pH on the removal of fluoride from water by FMSPs was investigated by varying the pH from 2, 3, 4, 5, 6, 7, 8, 9 to 10. The results are shown in Figure 4.6.

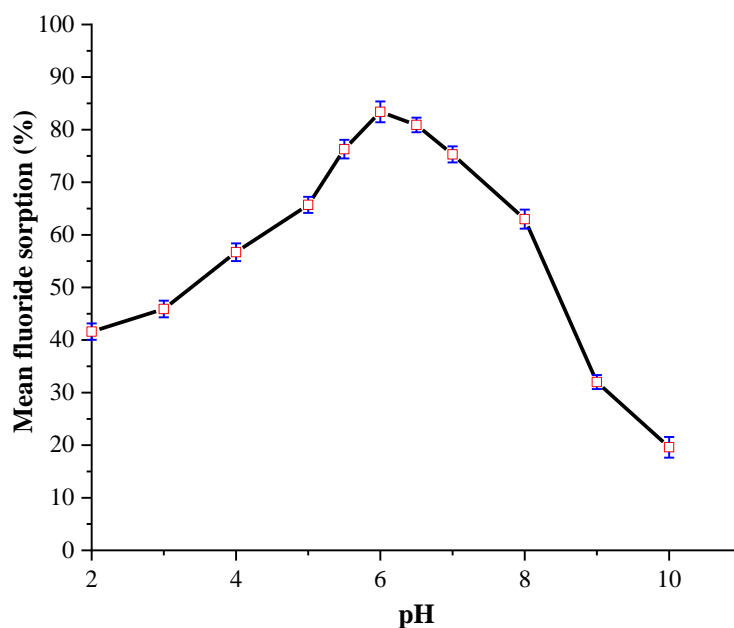


Figure 4.6: Effect of pH on the Adsorption Capacity of FMSPs

As illustrated in Figure 4.6, fluoride sorption increased from 41.6 % at pH 2 to an optimum of 83.4 % at pH 6 and then decreased as pH increased further. The pH of the solution is an important parameter in the adsorption process since it regulates the sorbent's surface charge and the degree of ionization of the adsorbate (Bibi *et al.*, 2015). The reduced sorption capacity at low pH could be due to the generation of weakly ionizing hydrofluoric acid, which decreases the availability of free fluoride ions for electrostatic interactions with Fe^{3+} on the sorbent surface (Bibi *et al.*, 2015; Kebede *et al.*, 2016). The decline in sorption capacity from 83.4 to 19.6 % when pH increased from 6 - 10 may be attributed to competition for the active site on the adsorbent between OH^- and F^- ions due to their similar ionic sizes and charges (Asgari *et al.*, 2012). Furthermore, the decrease in sorption capacity at alkaline pH can be due to the electrostatic repulsion of fluoride ions with the negatively charged adsorbent surface (Sharma *et al.*, 2021).

4.4.2 Effect of sorbent dose

The effect of sorbent dose on defluoridation was investigated by varying the sorbent dosage from 0.2, 0.4, 0.6, 0.8, 1.0, 1.5, 2.0 to 2.5 g at the optimal pH of 6. Figure 4.7 depicts the outcomes.

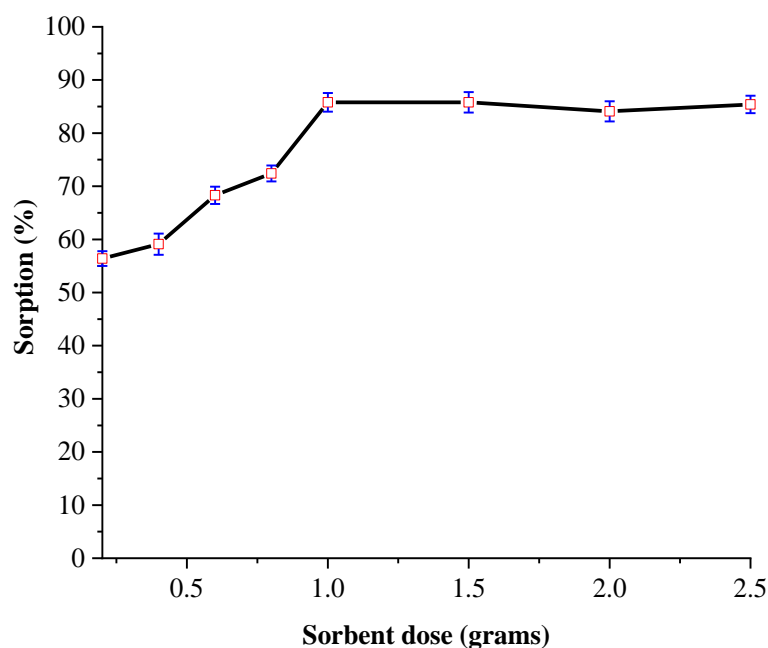


Figure 4.7: Effect of Sorbent Dose on the Adsorption Capacity of FMSPs

The results show that increasing the sorbent dose from 0.2 to 1.0 g increases fluoride removal from 56.4 to 85.8 % as in Figure 4.7. This may be attributed to the availability of a greater number of unoccupied active sorption sites and the existence of more surface areas for sorption (Kariuki *et al.*, 2017). However, increasing the sorbent dose from 1.0 to 2.5 g has no discernible effect on sorption capacity, presumably due to sorbent agglomeration or overlap, which reduces the availability of active sorption sites at higher sorbent doses (Cai *et al.*, 2015). In earlier studies, most adsorbents showed a similar trend (Kariuki *et al.*, 2017; Sadhu *et al.*, 2022).

4.4.3 Effect of Contact Time

The effect of time on fluoride uptake was studied at room temperature using optimum pH (6) and sorbent dose (1 g) by varying contact time from 5, 10, 15, 20, 25, 30, 35, 40, 45, 50, 60 to 90 minutes with 250 mL of 20 mg/L initial fluoride concentration. The results are depicted in Figure 4.8.

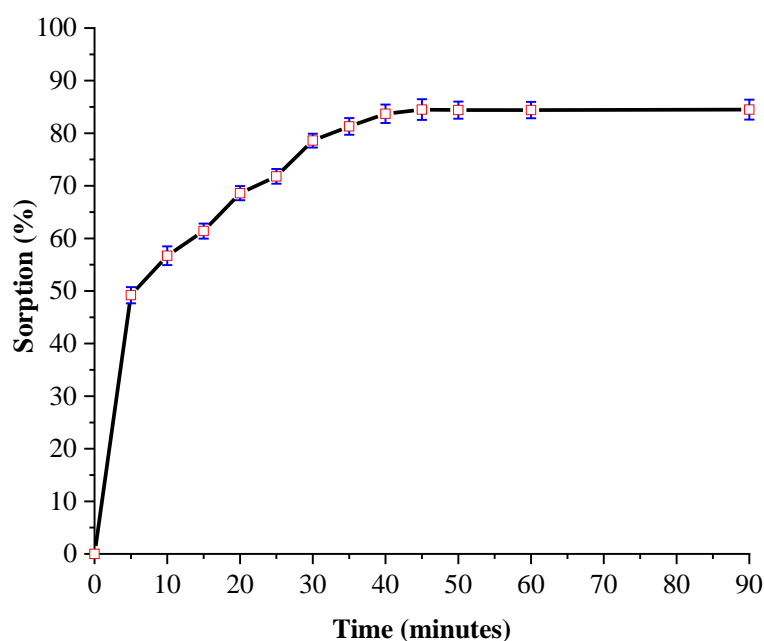


Figure 4.8: Effect of Contact Time on the Adsorption Capacity of FMSPs

Fluoride sorption increased rapidly in the beginning, from 49.2 to 84.5 % at 5 and 45 minutes (Figure 4.8). The presence of a higher number of vacant active sites and a fluoride concentration gradient may be responsible for the initial high fluoride sorption rate (Bibi *et al.*, 2015). After 45 minutes, there were negligible changes in fluoride uptake, presumably due to a decrease in the number of active sites and fluoride concentration (Sadhu *et al.*, 2022).

4.4.4 Effect of Initial Fluoride Concentration

The effect of initial fluoride concentration on fluoride removal was investigated at room temperature by varying the initial fluoride concentration from 2.5, 5, 10, 15,

20, 30, 40, 50 to 60 mg/L using the optimum pH (6), sorbent dose (1 g) and contact time (45 minutes). Figure 4.9 depicts the outcomes.

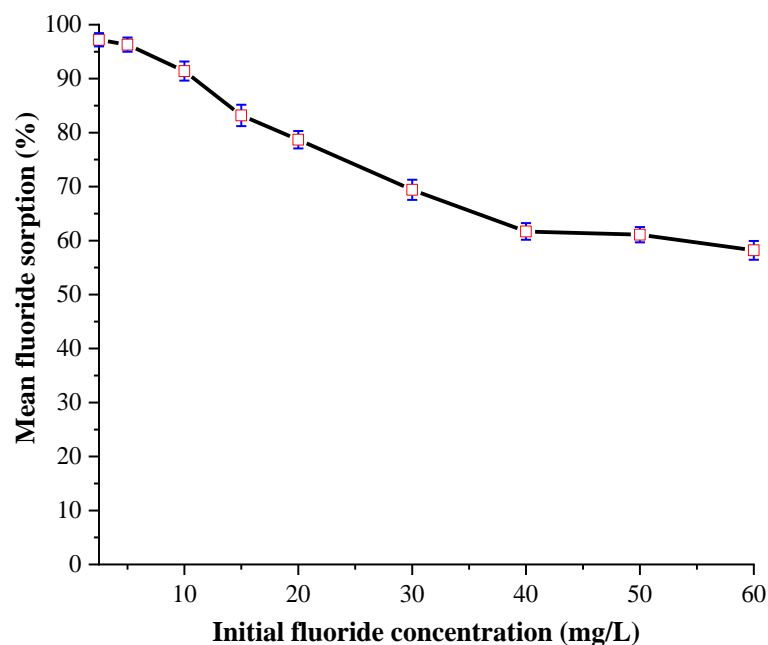


Figure 4.9: Effect of Initial Concentration on the Sorption Capacity of FMSPs

Fluoride adsorption is greater when the initial fluoride concentration is lower than when the initial fluoride concentration is higher (Figure 4.9). This means that the sorbent's capability diminishes as the initial fluoride concentrations rise. This could be ascribed to sorbent active site saturation as a result of a larger fluoride-to-sorbent active site ratio (Tomar *et al.*, 2014). Previous research has also shown that as the initial fluoride concentration increases, the sorbent's fluoride removal ability diminishes (Akafu *et al.*, 2019; Pillai, Dharaskar, Shah, *et al.*, 2020).

4.4.5 The Effect of Modification of Silica Particles with Iron on Fluoride Removal

The effect of modifying silica particles with $\text{Fe}(\text{NO}_3)_3 \cdot 9\text{H}_2\text{O}$ on fluoride removal was studied by comparing the adsorption capacities of unmodified silica particles with Fe-modified silica particles of different concentrations (0.2, 0.4, 0.6, 0.8, 1.0, 1.5 and

2 % w/w) at room temperature using optimum pH (6), sorbent dose (1 g) and contact time (45 minutes) with 20 mg/L fluoride solution. Figure 4.10 shows the results.

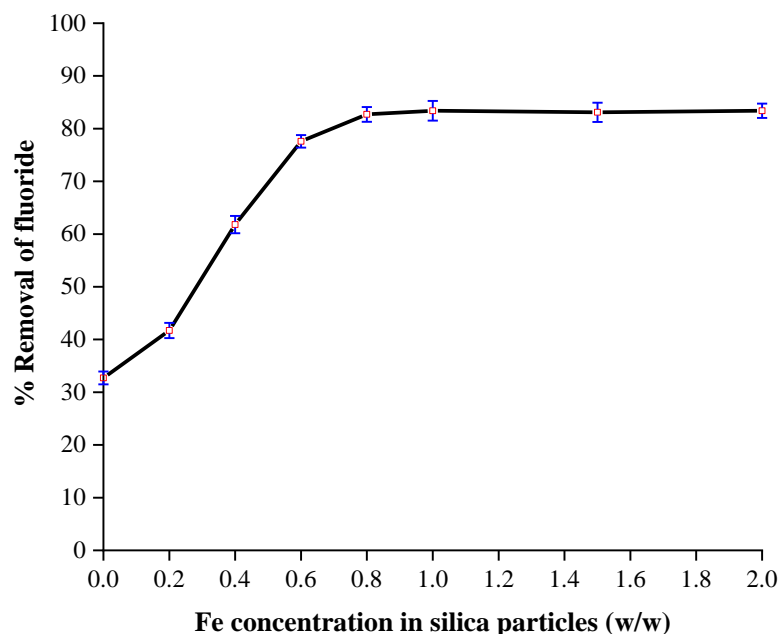


Figure 4.10: Effect of Modifying Silica Particles with Iron on Fluoride Removal

Unmodified silica particles have a low fluoride adsorption capacity (32.7 %), as shown in Figure 4.10. However, after modification, fluoride uptake increased with increasing iron concentration from 41.7 % (0.2 w/w) to 83.4 % (1 w/w). This is due to the increased Fe^{3+} concentration on the sorbent surface providing more active sites for F^- binding. However, the fluoride removal efficiency was found to be negligible as iron concentrations increased beyond 1 w/w, which was considered the optimum. According to the concept of hard and soft acids and bases (HSAB), Fe^{3+} is a hard acid, whereas F^- is a hard base, and hard acids have a high affinity for hard bases (Salifu *et al.*, 2013). As a result, it is the modification of silica particles with iron that resulted in increased fluoride removal efficiency.

4.4.6 Adsorption Isotherms

The Freundlich and Langmuir models were used to interpret the data from the adsorption experiment. The plots are presented in Figures 4.11 and 4.12, respectively.

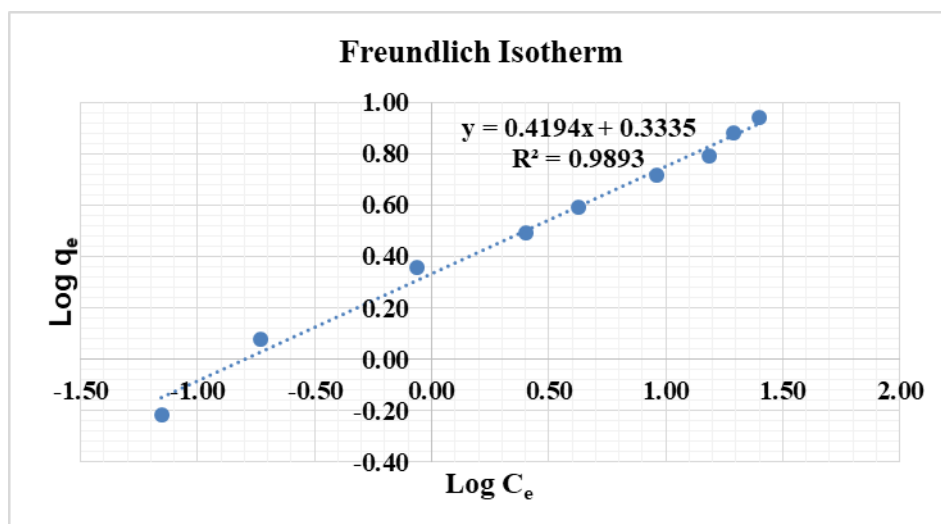


Figure 4.11: Freundlich Isotherm Plot for Defluoridation Using FMSPs

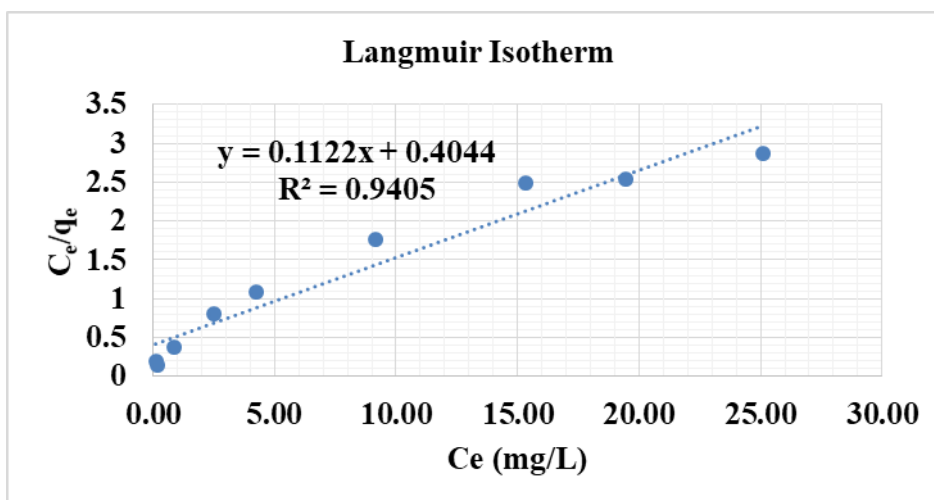


Figure 4.12: Langmuir Isotherm Plot for Defluoridation Using FMSPs

Table 4.6 shows that the experimental data fit better to the Freundlich isotherm model ($R^2 = 0.989$) than the Langmuir isotherm ($R^2 = 0.941$). The values of $1/n$ (0.419) between 0.1 and 1.0 and n (2.384) between 1-10 confirmed the high bond strength between the adsorbate and adsorbent, as well as the heterogeneous nature of the adsorbent surface. Furthermore, the low value of $1/n$ indicates the heterogeneity of the adsorbent surface (Rafique *et al.*, 2013). The small value of the Langmuir constant (K_L), 0.277 L/mg, implies a low heat of adsorption (Kofa *et al.*, 2017). The R_L value of 0.15 (Table 4.6), which is between 0 and 1, indicates favorable experimental conditions for sorption. Based on the Langmuir model, q_{max} is 8.913 mg/g (Table 4.6).

Table 4.6: Calculated Freundlich and Langmuir Isotherm Parameters

| Freundlich isotherm | | | | |
|----------------------------|------------|-------|-------|-------|
| Intercept | Slope(1/n) | N | K_F | R^2 |
| 0.334 | 0.419 | 2.384 | 2.155 | 0.989 |
| Langmuir isotherm | | | | |

| Intercept | Slope | $q_{\max}(\text{mg/g})$ | $K_L (\text{L/mg})$ | R^2 | R_L |
|-----------|-------|-------------------------|---------------------|-------|-------|
| 0.404 | 0.112 | 8.913 | 0.277 | 0.941 | 0.15 |

4.4.7 Kinetics of Defluoridation

In this study, the rate as well as the mechanism of defluoridation was evaluated using pseudo-first-order and pseudo-second-order kinetics models. The applicability of a particular model is based on the goodness of data fit (R^2). The linear plots for pseudo-first-order and pseudo-second-order models are presented in Figures 4.13 and 4.14, respectively.

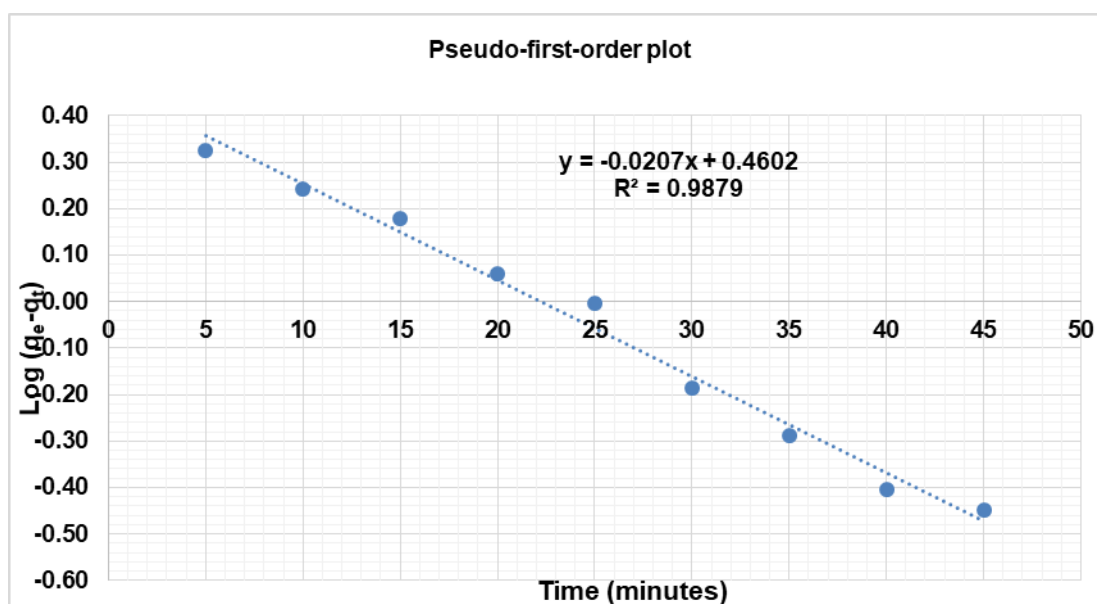


Figure 4.13: Pseudo-First-Order Kinetics Plot for Defluoridation Using FMSPs

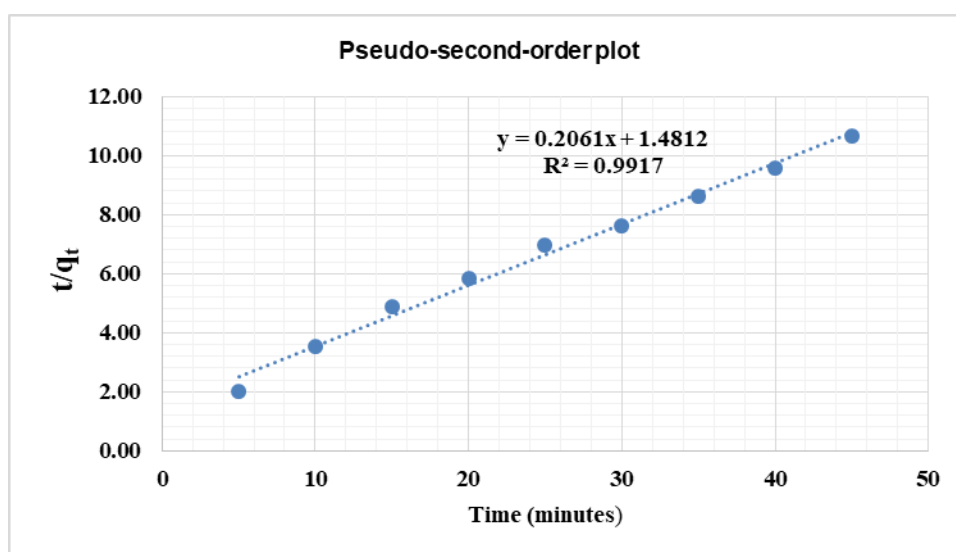


Figure 4.14: Pseudo-Second-Order Kinetics Plot for Defluoridation Using FMSPs

The linear regression plots show that the experimental data fit best to the pseudo-second-order model, which has a higher correlation coefficient of $R^2 = 0.992$ (Table 4.7), than the pseudo-first-order model ($R^2 = 0.988$).

Table 4.7: Kinetics Models Constants

| Pseudo-first-order | | | | | Pseudo-second-order | | | | |
|--------------------|-------|-----------|-------|-------|---------------------|-------|-----------|-------|-------|
| Slope | K_1 | Intercept | q_e | R^2 | Slope | q_e | Intercept | K_2 | R^2 |
| -0.021 | 0.048 | 0.460 | 2.885 | 0.988 | 0.206 | 4.852 | 1.481 | 0.029 | 0.992 |

The fit of this data to a pseudo-second-order model shows that adsorption occurs predominantly via chemisorption due to electrostatic attractions or, more likely, ion exchange processes (Akafu *et al.*, 2019; Yu *et al.*, 2013). These findings are consistent with the majority of previous studies on fluoride removal using various adsorbents, as shown in Table 4.8.

Table 4.8: Comparison of Efficiency of FMSPs with Different Adsorbents

| Adsorbent | pH | Kinetic model | Isotherm model | Adsorption capacity (mg/g) | Reference |
|---|-----------|----------------------|-----------------------|-----------------------------------|-------------------------------|
| Diatomite modified with Al(OH) ₃ | 6.7 | Pseudo-second-order | Freundlich | 1.7 | (Akafu <i>et al.</i> , 2019) |
| Nano silica from rice husk | 8.0 | Pseudo-second-order | Freundlich | 12.0 | (Pillai <i>et al.</i> , 2020) |
| Al(OH) ₃ loaded zeolite from fly ash | 6.0 | Pseudo-second-order | Langmuir | 18.1 | (Chen <i>et al.</i> , 2022) |
| Fired clay pots | 8.0 | Pseudo-second-order | Freundlich | 1.6 | (Kofa <i>et al.</i> , 2017) |
| Natural clay (Kaolinite) | 6.0 | Pseudo-second-order | Freundlich | 3.7 | (Nabbou <i>et al.</i> , 2019) |
| Marble waste powder | 7.0 | Pseudo-second-order | Freundlich | 1.2 | (Mehta <i>et al.</i> , 2016) |
| FMSPs | 6.0 | Pseudo-second-order | Freundlich | 8.9 | Current study |

4.5 Application of FMSPs to Real Water Samples

Water samples collected from Tiaty Baringo County in Kenya were utilized to examine the efficacy of FMSPs in defluoridation; the findings are displayed in Figure 4.15.

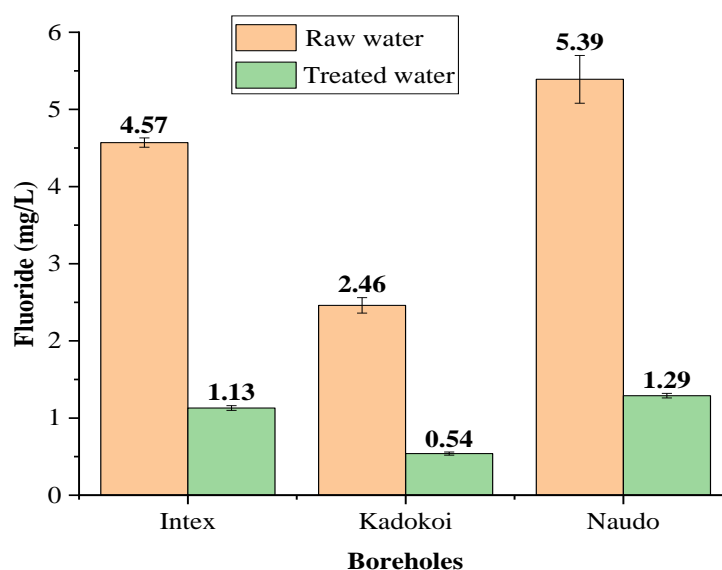


Figure 4.15: Comparison of Fluoride Levels in Raw and Treated Groundwater

Fluoride levels in borehole water decreased significantly up to the WHO criterion of 1.5 mg/L (WHO, 2017); Intex 4.57 ± 0.06 to 1.13 ± 0.03 (75.27 %), Kadokoi 2.46 ± 0.1 to 0.54 ± 0.02 (78.05 %), and Naudo 5.39 ± 0.31 to 1.2 ± 0.03 mg/L (77.74 %) as in Figure 4.15. However, the percentage of fluoride removal was lower than what could be obtained using the model solution, which is ascribed to competition for the sorbent active sites with other potential anions commonly found in groundwater such as Cl^- , SO_4^{2-} and HCO_3^- as shown in Table 4.2.

4.6 Regeneration Studies

Five cycles of adsorption-desorption experiments were performed using 0.1 M NaOH as a desorbing agent to evaluate the adsorbent's ability to be regenerated and

reused. The spent sorbent was soaked in NaOH for 2 hours, washed with deionized water until the pH of the washed water was 7, and dried in an oven at 90 °C for 4 hours. A fluoride solution of 20 mg/L was used, with an optimal sorbent dose (1 g) and contact time (45 minutes). Figure 4.16 depicts the results.

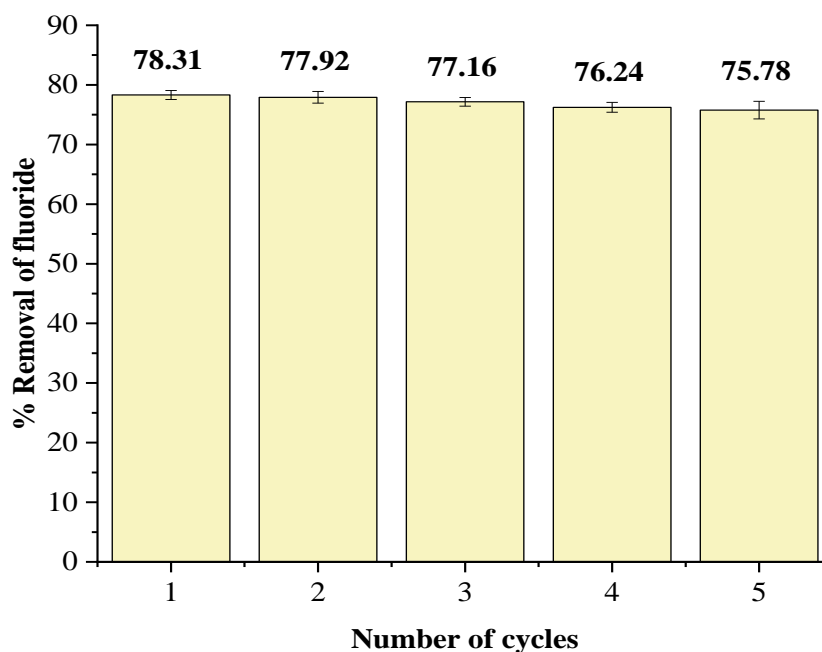


Figure 4.16: Regeneration of Fe-Modified Silica Particles (FMSPs)

The adsorption efficiency decreased with the number of cycles, but not significantly. This implies that the adsorbent can be recycled several times without losing its efficiency, which is an important factor to consider when choosing an adsorbent.

CHAPTER FIVE

CONCLUSIONS AND RECOMMENDATIONS

5.1 Conclusions

In this study, silica-based defluoridation sorbent was prepared by isolating silica particles from pumice rock via alkaline leaching. Its surface was modified with iron to increase selectivity towards fluoride, and used to evaluate fluoride removal from water. The following conclusions can be drawn from the study;

The temperature, pH, EC, and TDS values were in the range; 27.4 - 40.7 °C, 6.8 - 8.7, 402.89 - 4212.99 $\mu\text{S}/\text{cm}$, and 201.24 - 2111.77 mg/L, respectively. whereas the major ions levels were as follows: $\text{HCO}_3^- > \text{Na}^+ > \text{Cl}^- > \text{SO}_4^{2-} > \text{Mg}^{2+} > \text{Ca}^{2+} > \text{K}^+ > \text{F}^-$. Fluoride levels in the borehole water varied from 0.88 - 16.47 mg/L, with Intex, Riong'o, Kadokoi and Naudo boreholes exceeding the WHO standard of 1.5 mg/L. This was attributed to weathering of fluoride-rich minerals in volcanic bedrock.

The primary components of pumice rock were SiO_2 (61.41 ± 0.19 %), Al_2O_3 (12.07 ± 0.24 %), and Fe_2O_3 (11.06 ± 0.63 %). The extracted silica was 97.71 ± 0.19 % pure and amorphous, whereas the iron-functionalized silica particles contained 93.67 ± 0.66 % SiO_2 and 2.93 ± 0.02 % Fe_2O_3 .

The optimal pH, sorbent dose, and contact time for defluoridation using initial fluoride concentration of 20 mg/L were 6, 1 g, and 45 minutes, respectively. Fluoride adsorption fitted the Freundlich's isotherm model, indicating multilayer fluoride adsorption on a heterogeneous surface, whereas defluoridation followed pseudo-second-order kinetics, implying chemisorption.

The maximum fluoride removal efficiency in model solutions was 85.82 % under optimal conditions, with an adsorption capacity of 8.91 mg/g. The mean percentage removal efficiency in real samples was 77.02 %. The lower percentage removal in real water samples is attributed to matrix effects. The potential of the silica-based

sorbent developed from low-cost, abundant and locally available pumice rock in the removal of fluoride from water samples has been demonstrated.

5.2 Recommendations

1. Residents who use borehole water with high fluoride levels above 1.5 mg/L should be educated about fluoride's health effects and advised to use alternative safe sources.
2. To mitigate the negative health effects associated with elevated fluoride levels in drinking water, defluoridation of fluoride-rich borehole water is recommended by the use of low-cost sorbents such as iron-modified silica particles developed from pumice rock.
3. A cost-benefit analysis of the defluoridation sorbent developed from pumice volcanic rock is recommended to assess its economic viability.
4. Furthermore, this study recommends that more research be done on the effects of competing anions such as PO_4^{3-} , Cl^- , SO_4^{2-} , and NO_3^- on the efficiency of fluoride removal using iron-modified silica particles.

REFERENCES

- Addison, M. J., Rivett, M. O., Robinson, H., Fraser, A., Miller, A. M., Phiri, P., Mleta, P., & Kalin, R. M. (2020). Fluoride Occurrence in the Lower East African Rift System, Southern Malawi. *Science of the Total Environment*, 712, 1–16.
- Agarwal, S., Sadegh, H., Monajjemi, M., Salam, A., Ali, G. A. M., Memar, A. O. H., Shahryari-ghoshekandi, R., Tyagi, I., & Kumar, V. (2016). Efficient Removal of Toxic Bromothymol Blue and Methylene Blue from Wastewater by Polyvinyl Alcohol. *Journal of Molecular Liquids*, 218, 191–197.
- Ahmadijokani, F., Molavi, H., Rezakazemi, M., Aminabhavi, T. M., & Arjmand, M. (2021). Simultaneous Detection and Removal of Fluoride from Water using Smart Metal-Organic Framework-Based Adsorbents. *Coordination Chemistry Reviews*, 445, 214037.
- Akafu, T., Chimdi, A., & Gomoro, K. (2019). Removal of Fluoride from Drinking Water by Sorption using Diatomite Modified with Aluminum Hydroxide. *Journal of Analytical Methods in Chemistry*, 2019, 4831926.
- Akhtar, K., Khan, S. A., Khan, S. B., & Asiri, A. M. (2018). Scanning electron microscopy: Principle and applications in nanomaterials characterization. In *Handbook of Materials Characterization*.
- Alkurdi, S. S. A., Al-juboori, R. A., Bundschuh, J., & Hamawand, I. (2019). Bone Char as a Green Sorbent for Removing Health Threatening Fluoride from Drinking Water. *Environment International*, 127, 704–719.
- APHA. (2022). *Standard Methods for the Examination of Water and Wastewater* (24th ed.), Washington, DC, USA: American Public Health Association.
- Aregu, M. B., Asfaw, S. L., & Khan, M. M. (2018). Identification of Two Low Cost and Locally Available Filter Media (Pumice and Scoria) for Removal of Hazardous Pollutants from Tannery Wastewater. *Environmental Systems*

Research, 7(10), 1–14.

- Arulnangai, R., Mohamed Sihabudeen, M., Vivekanand, P. A., & Kamaraj, P. (2019). Influence of Physico Chemical Parameters on Potability of Ground Water in Ariyalur Area of Tamil Nadu, India. *Materials Today: Proceedings*, 36, 923–928.
- Asgari, G., Roshani, B., & Ghanizadeh, G. (2012). The Investigation of Kinetic and Isotherm of Fluoride Adsorption onto Functionalize Pumice Stone. *Journal of Hazardous Materials*, 217, 123–132.
- Bamigboye, C. O., Amao, J. A., Ayodele, T. A., Adebayo, A. S., Ogunleke, J. D., Abass, T. B., Oyedare, T. A., Adetutu, T. J., Adeeyo, A. O., & Oyedemi, A. A. (2020). An Appraisal of the Drinking Water Quality of Groundwater Sources in Ogbomoso, Oyo State, Nigeria. *Groundwater for Sustainable Development*, 11, 100453.
- Bibi, S., Farooqi, A., Hussain, K., & Haider, N. (2015). Evaluation of Industrial Based Adsorbents for Simultaneous Removal of Arsenic and Fluoride from Drinking Water. *Journal of Cleaner Production*, 87(1), 882–896.
- Bilici, M., & Pala, A. (2011). Removal of Arsenic from Drinking Water using Modified Natural Zeolite. *Desalination*, 281, 396–403.
- Biswas, G., Kumari, M., Adhikari, K., & Dutta, S. (2017). A Critical Review on Occurrence of Fluoride and its Removal through Adsorption with an Emphasis on Natural Minerals. *Current Pollution Reports*, 3(2), 104–119.
- Boadi, N. O., Saah, S. A., Baa-Poku, F., Mensah, E. A., & Addo, M. (2020). Safety of Borehole Water as an Alternative Drinking Water Source. *Scientific African*, 10, e00657.
- Borgohain, X., Boruah, A., Sarma, G. K., & Rashid, M. H. (2020). Rapid and Extremely High Adsorption Performance of Porous MgO Nanostructures for

Fluoride Removal from Water. *Journal of Molecular Liquids*, 305, 112799.

Brahman, K. D., Kazi, T. G., Afridi, H. I., Naseem, S., Arain, S. S., & Ullah, N. (2013). Evaluation of High Levels of Fluoride, Arsenic Species and other Physicochemical Parameters in Underground Water of two Sub Districts of Tharparkar, Pakistan: A Multivariate Study. *Journal of Water Research*, 47(3), 1005–1020.

Bratovčić, A., & Čatić, S. (2009). The Advantages of the use of Ion- Selective Potentiometry in Relation to UV / VIS Spectroscopy. *Agriculturae Conspectus Scientificus*, 74(3), 139–142.

Cai, H. M., Chen, G. J., Peng, C. Y., Zhang, Z. Z., Dong, Y. Y., Shang, G. Z., Zhu, X. H., Gao, H. J., & Wan, X. C. (2015). Removal of Fluoride from Drinking Water using Tea Waste Loaded with Al/Fe Oxides: A Novel, Safe and Efficient Biosorbent. *Applied Surface Science*, 328, 34–44.

Chebet, E. B., Kibet, J. K., & Mbui, D. (2020). The Assessment of Water Quality in River Molo Water Basin, Kenya. *Applied Water Science*, 10(4), 1–10.

Chen, J., Yang, R., Zhang, Z., & Wu, D. (2022). Removal of Fluoride from Water using Aluminum Hydroxide-Loaded Zeolite Synthesized from Coal Fly Ash. *Journal of Hazardous Materials*, 421, 126817.

Cherukumilli, K., Maurer, T., Hohman, J. N., Mehta, Y., & Gadgil, A. J. (2018). Effective Remediation of Groundwater Fluoride with Inexpensively Processed Indian Bauxite. *Environmental Science and Technology*, 52(8), 4711–4718.

Diagboya, P. N. E., & Dikio, E. D. (2018). Silica-Based Mesoporous Materials: Emerging Designer Adsorbents for Aqueous Pollutants Removal and Water Treatment. *Microporous and Mesoporous Materials*, 266, 252–267.

El-Moselhy, M. M., Ates, A., & Çelebi, A. (2017). Synthesis and Characterization of Hybrid Iron Oxide Silicates for Selective Removal of Arsenic Oxyanions from

Contaminated Water. *Journal of Colloid and Interface Science*, 488, 335–347.

Fuoco, I., Apollaro, C., Criscuoli, A., De Rosa, R., Velizarov, S., & Figoli, A. (2021). Fluoride Polluted Groundwaters in Calabria Region (Southern Italy): Natural Source and Remediation. *Water*, 13(12), 1–15.

Gai, W., & Deng, Z. (2021). A Comprehensive Review of Adsorbents for Fluoride Removal from Water: Performance, Water Quality Assessment and Mechanism. *Environmental Science Water Research & Technology*, 7(8), 1362–1386.

Ganvir, V., & Das, K. (2011). Removal of Fluoride from Drinking Water using Aluminum Hydroxide Coated Rice Husk Ash. *Journal of Hazardous Materials*, 185(2–3), 1287–1294.

Gevera, P., & Mouri, H. (2018). Natural Occurrence of Potentially Harmful Fluoride Contamination in Groundwater: An Example from Nakuru County, The Kenyan Rift Valley. *Environmental Earth Sciences*, 1–19.

Ghosh, S., Malloum, A., Igwegbe, C. A., Ighalo, J. O., Ahmadi, S., Dehghani, M. H., Othmani, A., Gökkuş, Ö., & Mubarak, N. M. (2022). New Generation Adsorbents for The Removal of Fluoride from Water and Wastewater: A Review. *Journal of Molecular Liquids*, 346.

Gisi, S. De, Lofrano, G., Grassi, M., & Notarnicola, M. (2016). Characteristics and Adsorption Capacities of Low-Cost Sorbents for Wastewater Treatment: A Review. *Sustainable Materials and Technologies*, 9, 10–40.

Glu, T., Kartal, S., & Sahin, U. (2004). Determination of Fluoride in Various Samples and Some Infusions using a Fluoride Selective Electrode. *Turkish Journal of Chemistry*, 28(2), 203–211.

Gogoi, C., Saikia, J., & Sarmah, S. (2018). Removal of Fluoride from Water by Locally Available Sand Modified with a Coating of Iron Oxides. *Water, Air, & Soil Pollution*, 229(4), 1–16.

- Habuda-Stanić, M., Ravančić, M. E., & Flanagan, A. (2014). A Review on Adsorption of Fluoride from Aqueous Solution. *Materials*, 7, 6317–6366.
- Hasan, M. K., Shahriar, A., & Jim, K. U. (2019). Water Pollution in Bangladesh and its Impact on Public Health. *Heliyon*, 5(8), e02145.
- He, J., Yang, Y., Wu, Z., Xie, C., Zhang, K., Kong, L., & Liu, J. (2020). Review of Fluoride Removal from Water Environment by Adsorption. *Journal of Environmental Chemical Engineering*, 8(6), 104516.
- Heibati, B., Rodriguez-couto, S., Amrane, A., Rafatullah, M., Hawari, A., & Al-ghouti, M. A. (2014). Uptake of Reactive Black 5 by Pumice and Walnut Activated Carbon: Chemistry and Adsorption Mechanisms. *Journal of Industrial and Engineering Chemistry*, 20(5), 2939–2947.
- Imoisili, P. E., Ukoba, K. O., & Jen, T. C. (2020). Green Technology Extraction and Characterization of Silica Nanoparticles from Palm Kernel Shell Ash via Sol-Gel. *Journal of Materials Research and Technology*, 9(1), 307–313.
- Ismail, A. I. M., El-Shafey, O. I., Amr, M. H. A., & El-Maghraby, M. S. (2014). Pumice Characteristics and their Utilization on the Synthesis of Mesoporous Minerals and on the Removal of Heavy Metals. *International Scholarly Research Notices*, 2014, 1–9.
- Jagtap, S., Yenkie, M. K., Labhsetwar, N., & Rayalu, S. (2012). Fluoride in Drinking Water and Defluoridation of Water. *Chemical Reviews*, 2454–2466.
- Kalam, S., Abu-Khamsin, S. A., Kamal, M. S., & Patil, S. (2021). Surfactant Adsorption Isotherms: A Review. *ACS Omega*, 6(48), 32342–32348.
- Karande, S. D., Jadhav, S. A., Garud, H. B., Kalantre, V. A., Burungale, S. H., & Patil, P. S. (2021). Green and Sustainable Synthesis of Silica Nanoparticles. *Nanotechnology for Environmental Engineering*, 6(2), 1–14.

- Kariuki, Z., Kiptoo, J., & Onyancha, D. (2017). Biosorption Studies of Lead and Copper using Rogers Mushroom Biomass 'Lepiota hystrix.' *South African Journal of Chemical Engineering*, 23, 62–70.
- Karthika, I. N., Thara, K., & Dheenadayalan, M. S. (2018). Physico-Chemical Study of the Ground Water Quality at Selected Locations in Periyakulam, Theni District, Tamilnadu, India. *Materials Today: Proceedings*, 5(1), 422–428.
- Kebede, B., Beyene, A., Fufa, F., Megersa, M., & Behm, M. (2016). Experimental Evaluation of Sorptive Removal of Fluoride from Drinking Water using Iron Ore. *Applied Water Science*, 6(1), 57–65.
- Kimambo, V., Bhattacharya, P., Mtaló, F., Mtamba, J., & Ahmad, A. (2019). Groundwater for Sustainable Development Fluoride Occurrence in Groundwater Systems at Global Scale and Status of Defluoridation – State of the Art. *Groundwater for Sustainable Development*, 9, 100223.
- Kofa, G. P., Gomdje, V. H., Telegang, C., & Koungou, S. N. (2017). Removal of Fluoride from Water by Adsorption onto Fired Clay Pots: Kinetics and Equilibrium Studies. *Journal of Applied Chemistry*, 2017, 1–7.
- Kut, K. M. K., Sarswat, A., Srivastava, A., Pittman, C. U., & Mohan, D. (2016). A Review of Fluoride in African Groundwater and Local Remediation Methods. *Groundwater for Sustainable Development*, 2–3, 190–212.
- Lin, K. Y. A., Liu, Y. T., & Chen, S. Y. (2016). Adsorption of Fluoride to UiO-66-NH₂ in Water: Stability, Kinetic, Isotherm and Thermodynamic Studies. *Journal of Colloid and Interface Science*, 461, 79–87.
- Malago, J., Makoba, E., & Muzuka, A. N. N. (2017). Fluoride Levels in Surface and Groundwater in Africa: A Review. *American Journal of Water Science and Engineering*, 3(1), 1–17.
- Meenakshi, & Maheshwari, R. C. (2006). Fluoride in Drinking Water and its Removal.

Journal of Hazardous Materials, 137(1), 456–463.

Mehta, D., Mondal, P., & George, S. (2016). Utilization of Marble Waste Powder as a Novel Adsorbent for Removal of Fluoride Ions from Aqueous Solution. *Journal of Environmental Chemical Engineering*, 4(1), 932–942.

Meride, Y., & Ayenew, B. (2016). Drinking Water Quality Assessment and its Effects on Residents Health in Wondo Genet Campus, Ethiopia. *Environmental Systems Research*, 5(1), 1–7.

Mohapatra, M., Anand, S., Mishra, B. K., Giles, D. E., & Singh, P. (2009). Review of Fluoride Removal from Drinking Water. *Journal of Environmental Management*, 91(1), 67–77.

Mohseni-Bandpei, A., Eslami, A., Kazemian, H., Zarrabi, M., & Al-Musawi, T. J. (2020). A High Density 3-Aminopropyltriethoxysilane Grafted Pumice-Derived Silica Aerogel as an Efficient Adsorbent for Ibuprofen: Characterization and Optimization of the Adsorption Data using Response Surface Methodology. *Environmental Technology & Innovation*, 18, 100642.

Mourhly, A., Hamidi, A. El, Halim, M., & Aarsalane, S. (2015). The Synthesis and Characterization of Low-Cost Mesoporous Silica SiO₂ from Local Pumice Rock. *Nanomaterials and Nanotechnology*, 5, 35.

Mourhly, A., Jhilal, F., El Hamidi, A., Halim, M., & Aarsalane, S. (2019). Highly Efficient Production of Mesoporous Nano-Silica from Unconventional Resource: Process Optimization using a Central Composite Design. *Microchemical Journal*, 145, 139–145.

Murambasvina, G., & Mahamadi, C. (2020). Effective Fluoride Adsorption using Water Hyacinth Beads Doped with Hydrous Oxides of Aluminium and Iron. *Groundwater for Sustainable Development*, 10, 100302.

Mutonga, M. (2014). Fluoride Ions in Groundwater Case Study; Baringo - Bogoria

Geothermal Area in Kenya. *5th African Rift Geothermal Conference Arusha, Tanzania, 29-31 October 2014*, 1–10.

Mwiathi, N. F., Gao, X., Li, C., & Rashid, A. (2022). The Occurrence of Geogenic Fluoride in Shallow Aquifers of Kenya Rift Valley and its Implications in Groundwater Management. *Ecotoxicology and Environmental Safety*, 229, 113046.

Nabbou, N., Belhachemi, M., Boumelik, M., Merzougui, T., Lahcene, D., Harek, Y., Zorpas, A. A., & Jeguirim, M. (2019). Removal of Fluoride from Groundwater using Natural Clay (Kaolinite): Optimization of Adsorption Conditions. *Comptes Rendus Chimie*, 22(2–3), 105–112.

Nayak, P., & Datta, A. (2021). Synthesis of SiO₂-Nanoparticles from Rice Husk Ash and its Comparison with Commercial Amorphous Silica through Material Characterization. *Silicon*, 13(4), 1209–1214.

Nehra, S., Raghav, S., & Kumar, D. (2020). Biomaterial Functionalized Cerium Nanocomposite for Removal of Fluoride using Central Composite Design Optimization Study. *Environmental Pollution*, 258, 113773.

Noori, M., Amrane, A., Aldin, K., Zarrabi, M., & Reza, H. (2014). Potential of Waste Pumice and Surface Modified Pumice for Hexavalent Chromium Removal: Characterization, Equilibrium, Thermodynamic and Kinetic Study. *Journal of the Taiwan Institute of Chemical Engineers*, 45(2), 635–647.

Ochieng, L., Kipng'ok, J., Kanda, I., Igunza, G., & Wanjie, C. (2012). Geochemistry of Fumarole Discharges and Borehole Waters of Korosi-Chepchuk Geothermal Prospect, Kenya. *Transactions - Geothermal Resources Council*, 36, 17–21.

Olaka, L. A., Wilke, F. D. H., Olago, D. O., Odada, E. O., Mulch, A., & Musolff, A. (2016). Groundwater Fluoride Enrichment in an Active Rift Setting: Central Kenya Rift Case Study. *Science of the Total Environment*, 545, 641–653.

- Pan, S. Y., Haddad, A. Z., & Gadgil, A. J. (2019). Toward Greener and More Sustainable Manufacture of Bauxite-Derived Adsorbents for Water Defluoridation. *ACS Sustainable Chemistry and Engineering*, 7(22), 18323–18331.
- Pillai, P., Dharaskar, S., & Pandian, S. (2020). Rice Husk Derived Silica Nano Doped on Calcium Peroxide for Fluoride: Performance, Characterization, Kinetic, Isotherm, and Groundwater treatment. *Environmental Technology and Innovation*, 19, 100901.
- Pillai, P., Dharaskar, S., Shah, M., & Sultania, R. (2020). Determination of Fluoride Removal using Silica Nano Adsorbent Modified by Rice Husk from Water. *Groundwater for Sustainable Development*, 11, 100423.
- Pillai, P., Kakadiya, N., Timaniya, Z., Dharaskar, S., & Sillanpaa, M. (2019). Removal of Arsenic using Iron Oxide Amended with Rice Husk Nanoparticles from Aqueous Solution. *Materials Today: Proceedings*, 28, 830–835.
- Prasanth, S. S., Magesh, N. S., Jitheshlal, K. V., Chandrasekar, N., & Gangadhar, K. (2012). Evaluation of Groundwater Quality and its Suitability for Drinking and Agricultural use in the Coastal Stretch of Alappuzha District, Kerala, India. *Applied Water Science*, 2(3), 165–175.
- Rafique, A., Awan, M. A., Wasti, A., Qazi, A. I., & Arshad, M. (2013). Removal of Fluoride from Drinking Water using Modified Immobilized Activated Alumina. *Journal of Chemistry*, 2013.
- Rasool, A., Xiao, T., Baig, Z. T., & Masood, S. (2015). Co-occurrence of Arsenic and Fluoride in the Groundwater of Punjab, Pakistan: Source Discrimination and Health Risk Assessment. *Environmental Science and Pollution Research*, 22(24), 19729–19746.
- Renu, Agarwal, M., & Singh, K. (2017). Heavy Metal Removal from Wastewater using Various Adsorbents: A Review. *Journal of Water Reuse and Desalination*, 7(4),

387–419.

- Rovani, S., Santos, J. J., Corio, P., & Fungaro, D. A. (2018). Highly Pure Silica Nanoparticles with High Adsorption Capacity Obtained from Sugarcane Waste Ash. *ACS Omega*, 3(3), 2618–2627.
- Rusiniak, P., Sekuła, K., Sracek, O., & Stopa, P. (2021). Fluoride Ions in Groundwater of the Turkana County, Kenya, East Africa. *Acta Geochimica*, 40(6), 945–960.
- Sadegh, H., Ali, G. A. M., & Gupta, V. K. (2017). The Role of Nanomaterials as Effective Adsorbents and their Applications in Wastewater Treatment. *Journal of Nanostructure in Chemistry*, 7(1), 1–14.
- Sadhu, M., Bhattacharya, P., Vithanage, M., & Padmaja Sudhakar, P. (2022). Adsorptive Removal of Fluoride using Biochar – A Potential Application in Drinking Water Treatment. *Separation and Purification Technology*, 278, 119106.
- Salifu, A., Petrusevski, B., Ghebremichael, K., Modestus, L., Buamah, R., Aubry, C., & Amy, G. L. (2013). Aluminum Hydroxide Coated Pumice for Fluoride Removal from Drinking Water: Synthesis, Equilibrium, Kinetics and Mechanism. *Chemical Engineering Journal*, 228, 63–74.
- Sekomo, C. B., Rousseau, D. P. L., & Lens, P. N. L. (2012). Use of Gisenyi Volcanic Rock for Adsorptive Removal of Cd (II), Cu (II), Pb (II), and Zn (II) from Wastewater. *Water, Air, and Soil Pollution*, 223(2), 533–547.
- Sharma, R., Sharma, R., Parveen, K., Pant, D., & Malaviya, P. (2021). Comprehensive and Critical Appraisal of Plant-Based Defluoridation from Environmental Matrices. *Chemosphere*, 281, 130892.
- Simiyu, S. M. (2010). Status of Geothermal Exploration in Kenya and Future Plans for its Development. *World Geothermal Congress 2010*, 25–29.

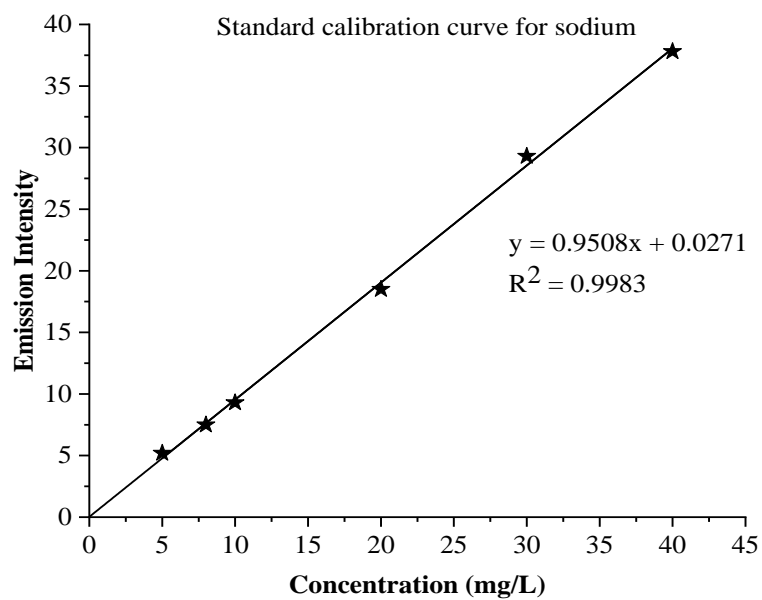
- Soleimani, H., Mahvi, A. H., Yaghmaeian, K., Abbasnia, A., Sharafi, K., Alimohammadi, M., & Zamanzadeh, M. (2019). Effect of Modification by Five Different Acids on Pumice Stone as Natural and Low-Cost Adsorbent for Removal of Humic Acid from Aqueous Solutions - Application of Response Surface Methodology. *Journal of Molecular Liquids*, 290, 111181.
- Srivastava, A., Kumari, M., Ramanathan, A., Selvaraj, K., Prasad, B., & Prasad, K. S. (2020). Removal of Fluoride from Aqueous Solution by Mesoporous Silica Nanoparticles Functionalized with Chitosan Derived from Mushroom. *Journal of Macromolecular Science, Part A: Pure and Applied Chemistry*, 57(9), 619–627.
- Stober, W., & Fink, A. (1967). Controlled Growth of Monodisperse Silica Spheres in the Micron Size Range. *Journal of Colloid and Interface Science*, 26, 62–69.
- Suneetha, M., Sundar, B. S., & Ravindhranath, K. (2015). Removal of Fluoride from Polluted Waters using Active Carbon Derived from Barks of Vitex Negundo Plant. *Journal of Analytical Science and Technology*, 6(1), 1–19.
- Tabi, R. N., Agyemang, F. O., Mensah-Darkwa, K., Arthur, E. K., Gikunoo, E., & Momade, F. (2021). Zeolite Synthesis and Its Application in Water Defluorination. *Materials Chemistry and Physics*, 261, 124229.
- Thakur, L. S., & Mondal, P. (2017). Simultaneous Arsenic and Fluoride Removal from Synthetic and Real Groundwater by Electrocoagulation Process: Parametric and Cost Evaluation. *Journal of Environmental Management*, 190, 102–112.
- Tomar, V., Prasad, S., & Kumar, D. (2013). Adsorptive Removal of Fluoride from Water Samples using Zr-Mn Composite Material. *Microchemical Journal*, 111, 116–124.
- Tomar, V., Prasad, S., & Kumar, D. (2014). Adsorptive Removal of Fluoride from Aqueous Media using Citrus limonum (Lemon) Leaf. *Microchemical Journal*, 112, 97–103.

- Udhayakumar, R., Manivannan, P., Raghu, K., & Vaideki, S. (2016). Assessment of Physico-Chemical Characteristics of Water in Tamilnadu. *Ecotoxicology and Environmental Safety*, 134, 474–477.
- Velazquez-jimenez, L. H., Vences-alvarez, E., Flores-arciniega, J. L., Flores-zuñiga, H., & Rangel-mendez, J. R. (2015). Water Defluoridation with Special Emphasis on Adsorbents-Containing Metal Oxides and / or Hydroxides: A Review. *Separation and Purification Technology*, 150, 292–307.
- Vijila, B., Gladis, E. H. E., Jose, J. M. A., Sharmila, T. M., & Joseph, J. (2021). Removal of Fluoride with Rice Husk Derived Adsorbent from Agro Waste Materials. *Materials Today: Proceedings*, 45, 2125–2129.
- Vinati, A., Mahanty, B., & Behera, S. K. (2015). Clay and Clay Minerals for Fluoride Removal from Water: A State-of-the-Art Review. *Applied Clay Science*, 114, 340–348.
- Wambu, E. W., Ambusso, W. O., Onindo, C., & Muthakia, G. K. (2016). Review of Fluoride Removal from Water by Adsorption using Soil Adsorbents – An Evaluation of The Status. *Journal of Water Reuse and Desalination*, 6(1), 1–29.
- Wan, K., Huang, L., Yan, J., Ma, B., Huang, X., Luo, Z., Zhang, H., & Xiao, T. (2021). Removal of Fluoride from Industrial Wastewater by using Different Adsorbents: A Review. *Science of the Total Environment*, 773, 145535.
- Wang, X., Zhang, Z., Zhao, Y., Xia, K., Guo, Y., Qu, Z., & Bai, R. (2018). A mild and Facile Synthesis of Amino Functionalized $\text{CoFe}_2\text{O}_4 @\text{SiO}_2$ for Hg(II) Removal. *Nanomaterials*, 8(9), 673.
- WHO. (2017). *Guidelines for Drinking-Water Quality* (4th ed.). Geneva: World Health Organization.
- WHO and UNICEF. (2021). *Progress on Household Drinking Water, Sanitation and Hygiene 2000-2020: Five Years into the SDGs*. Geneva: WHO and UNICEF.

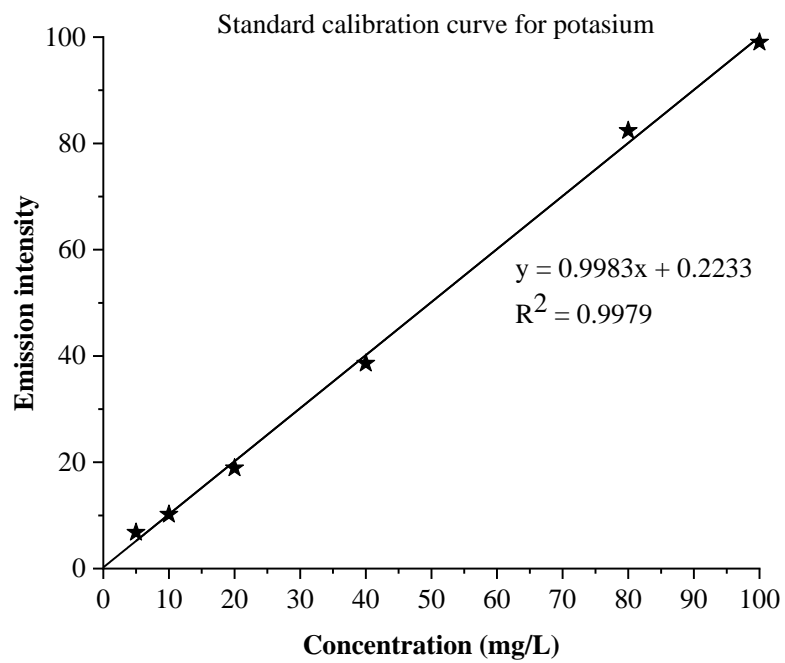
- Yadav, A. K., & Bhattacharyya, S. (2020). A Review of the Emerging Ceramic Adsorbents for Defluoridation of Groundwater. *Journal of Water Process Engineering*, 36, 101365.
- Yu, X., Tong, S., Ge, M., & Zuo, J. (2013). Removal of Fluoride from Drinking Water by Cellulose@Hydroxyapatite Nanocomposites. *Carbohydrate Polymers*, 92(1), 269–275.
- Zhang, C., Li, Y., Wang, T. J., Jiang, Y., & Fok, J. (2017). Synthesis and Properties of a High-Capacity Iron Oxide Adsorbent for Fluoride Removal from Drinking Water. *Applied Surface Science*, 425, 272–281.
- Zhang, L. P., Liu, Z., Faraj, Y., Zhao, Y., Zhuang, R., Xie, R., Ju, X. J., Wang, W., & Chu, L. Y. (2019). High-flux Efficient Catalytic Membranes Incorporated with Iron-based Fenton-like Catalysts for Degradation of Organic Pollutants. *Journal of Membrane Science*, 573, 493–503.
- Zulfiqar, U., Subhani, T., & Husain, S. W. (2016). Synthesis and Characterization of Silica Nanoparticles from Clay. *Journal of Asian Ceramic Societies*, 4(1), 91–96.

APPENDICES

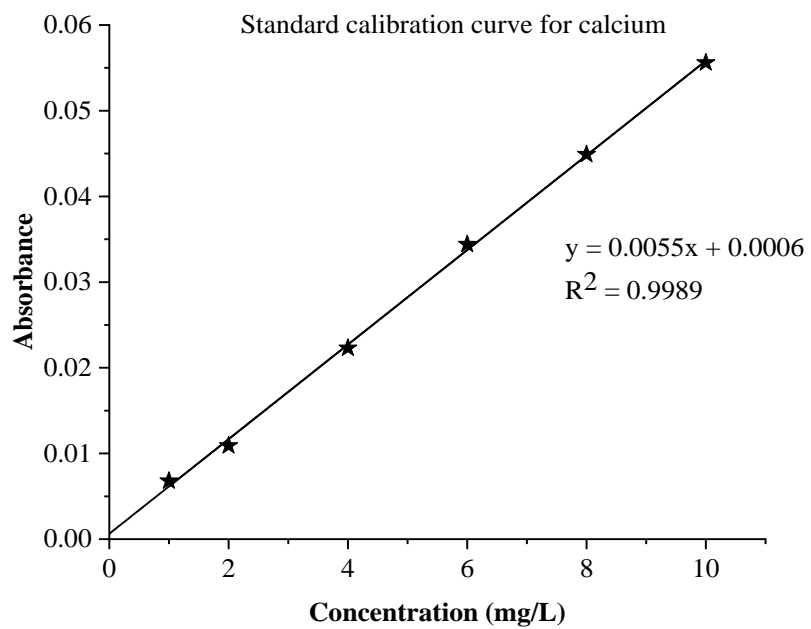
Appendix I: Standard Calibration Curve for Sodium



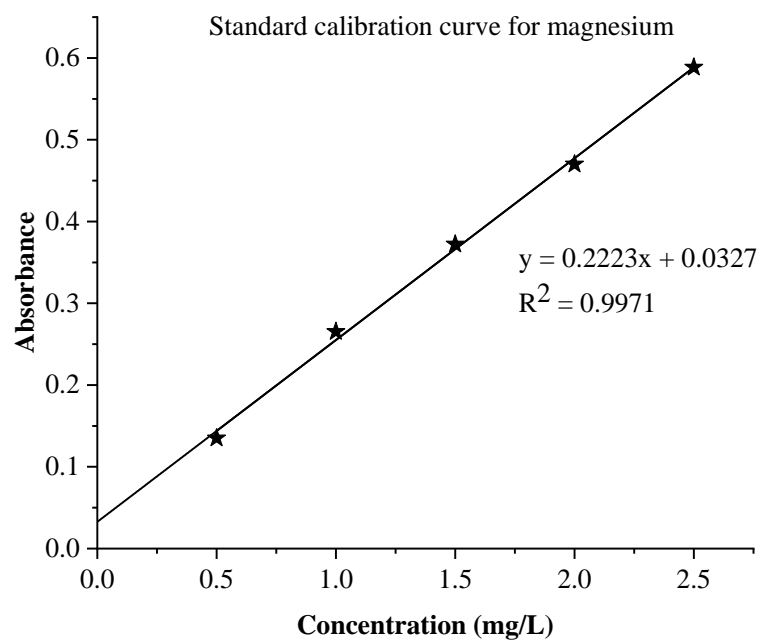
Appendix II: Standard Calibration Curve for Potassium



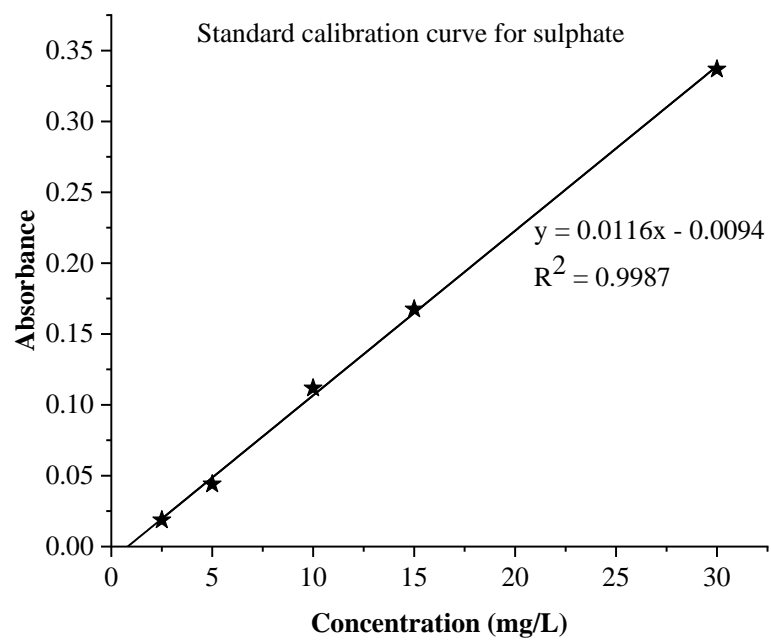
Appendix III: Standard Calibration Curve for Calcium



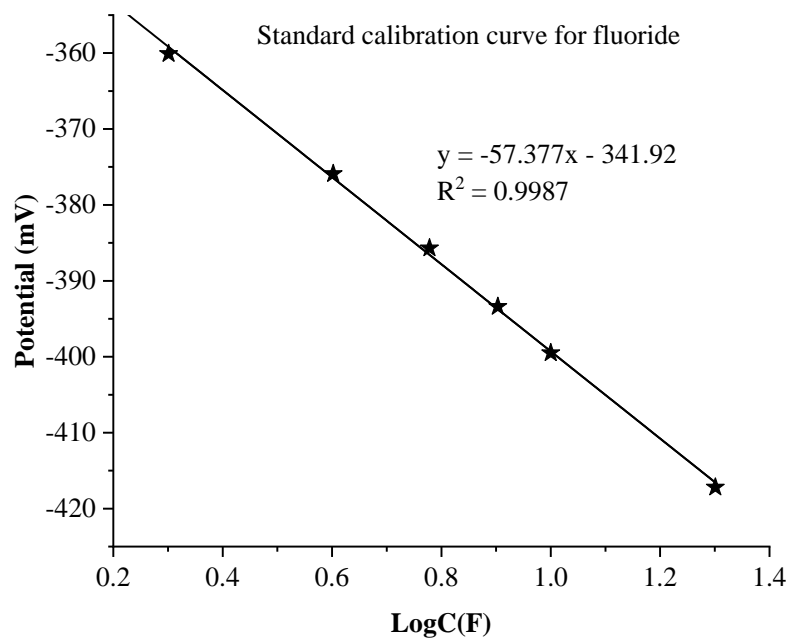
Appendix IV: Standard Calibration Curve for Magnesium



Appendix V: Standard Calibration Curve for Sulphate



Appendix VI: Standard Calibration Curve for Fluoride



Appendix VII: Percent Fluoride Removal at Different pH (Initial Fluoride Concentration = 20 mg/L, Sorbent Dose = 1.5 g, and Contact Time = 90 minutes)

| Ph | % Sorption |
|-----------|-------------------|
| 2.0 | 41.62 ± 1.55 |
| 3.0 | 45.94 ± 1.58 |
| 4.0 | 56.71 ± 1.68 |
| 5.0 | 65.69 ± 1.52 |
| 5.5 | 76.34 ± 1.78 |
| 6.0 | 83.38 ± 1.98 |
| 6.5 | 80.88 ± 1.40 |
| 7.0 | 75.33 ± 1.53 |
| 8.0 | 63.12 ± 1.81 |
| 9.0 | 32.41 ± 1.32 |
| 10.0 | 19.57 ± 1.96 |

Appendix VIII: Percent Fluoride Removal at Different Sorbent Doses (Initial Fluoride Concentration = 20 mg/L, pH = 6, and Contact Time = 90 Minutes)

| Dose (g) | % Sorption |
|-----------------|-------------------|
| 0.2 | 56.44 ± 1.39 |
| 0.4 | 59.12 ± 1.99 |
| 0.6 | 68.34 ± 1.63 |
| 0.8 | 72.41 ± 1.52 |
| 1.0 | 85.79 ± 1.76 |
| 1.5 | 85.82 ± 1.92 |
| 2.0 | 84.11 ± 1.89 |
| 2.5 | 85.39 ± 1.65 |

Appendix IX: Percent Fluoride Removal at Different Contact Times (Initial Fluoride Concentration = 20 mg/L, pH = 6 and Sorbent Dose = 1 g)

| Time (minutes) | % Sorption |
|-----------------------|-------------------|
| 5 | 49.23 ± 1.54 |
| 10 | 56.68 ± 1.78 |
| 15 | 61.41 ± 1.43 |
| 20 | 68.63 ± 1.35 |
| 25 | 71.81 ± 1.41 |
| 30 | 78.59 ± 1.32 |
| 35 | 81.32 ± 1.58 |
| 40 | 83.67 ± 1.76 |
| 45 | 84.54 ± 1.97 |
| 50 | 84.39 ± 1.63 |
| 60 | 84.43 ± 1.56 |
| 90 | 84.46 ± 1.89 |

Appendix X: Percent Fluoride Removal at Different Initial Fluoride Concentrations (pH = 6, Sorbent Dose = 1 g, and Contact Time = 45 Minutes)

| Initial fluoride concentration (mg/L) | % Sorption |
|--|-------------------|
| 2.5 | 97.18 ± 1.23 |
| 5.0 | 96.32 ± 1.31 |
| 10.0 | 91.37 ± 1.77 |
| 15.0 | 83.24 ± 1.98 |
| 20.0 | 78.67 ± 1.61 |
| 30.0 | 69.42 ± 1.87 |
| 40.0 | 61.73 ± 1.53 |
| 50.0 | 61.09 ± 1.41 |
| 60.0 | 58.17 ± 1.74 |

Appendix XI: Effect of Modification of SPs with Iron on Fluoride Removal

| Fe concentration in sorbent (w/w) | % Sorption |
|--|-------------------|
| 0 | 32.7 ± 1.22 |
| 0.2 | 41.7 ± 1.44 |
| 0.4 | 61.8 ± 1.65 |
| 0.6 | 77.6 ± 1.19 |
| 0.8 | 82.7 ± 1.41 |
| 1 | 83.4 ± 1.87 |
| 1.5 | 83.1 ± 1.83 |
| 2 | 83.4 ± 1.36 |

Appendix XII: Freundlich Isotherm Raw Data at Optimum Conditions

| Ce | Log Ce | qe | Log qe |
|-----------|---------------|-----------|---------------|
| 0.07 | -1.15 | 0.61 | -0.22 |
| 0.19 | -0.73 | 1.20 | 0.08 |
| 0.86 | -0.07 | 2.29 | 0.36 |
| 2.52 | 0.40 | 3.12 | 0.49 |
| 4.26 | 0.63 | 3.94 | 0.59 |
| 9.18 | 0.96 | 5.21 | 0.72 |
| 15.32 | 1.19 | 6.17 | 0.79 |
| 19.45 | 1.29 | 7.64 | 0.88 |
| 25.08 | 1.40 | 8.73 | 0.94 |

Appendix XIII: Langmuir Isotherm Raw Data at Optimum Conditions

| C_e (mg/L) | q_e (mg/g) | C_e/q_e |
|--------------|--------------|-----------|
| 0.07 | 0.61 | 0.12 |
| 0.19 | 1.20 | 0.15 |
| 0.86 | 2.29 | 0.38 |
| 2.52 | 3.12 | 0.81 |
| 4.26 | 3.94 | 1.08 |
| 9.18 | 5.21 | 1.76 |
| 15.32 | 6.17 | 2.48 |
| 19.45 | 7.64 | 2.55 |
| 25.08 | 8.73 | 2.87 |

Appendix XIV: Pseudo-First-Order Kinetics Raw Data at Optimum Conditions

| Time (min) | q_t (mg/g) | log (q_e-q_t) |
|-------------------|-----------------------------|--|
| 5 | 2.46 | 0.33 |
| 10 | 2.835 | 0.24 |
| 15 | 3.07 | 0.18 |
| 20 | 3.43 | 0.06 |
| 25 | 3.59 | 0.00 |
| 30 | 3.93 | -0.19 |
| 35 | 4.065 | -0.29 |
| 40 | 4.185 | -0.40 |
| 45 | 4.225 | -0.45 |

Appendix XV: Pseudo-Second-Order Kinetics Raw Data at Optimum Conditions

| Time (min) | q_t (mg/g) | t/q_t |
|-------------------|-----------------------------|------------------------|
| 5 | 2.46 | 2.03 |
| 10 | 2.84 | 3.53 |
| 15 | 3.07 | 4.89 |
| 20 | 3.43 | 5.83 |
| 25 | 3.59 | 6.96 |
| 30 | 3.93 | 7.63 |
| 35 | 4.07 | 8.61 |
| 40 | 4.19 | 9.56 |
| 45 | 4.23 | 10.65 |

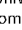


OPEN Iron functionalized silica particles as an ingenious sorbent for removal of fluoride from water

Paul Kiprono , Jackson Kiptoo, Eunice Nyawade & Elijah Ngumba

The paucity of safe drinking water remains a global concern. Fluoride is a pollutant prevalent in groundwater that has adverse health effects. To resolve this concern, we devised a silica-based defluoridation sorbent from pumice rock obtained from the Paka volcano in Baringo County, Kenya. The alkaline leaching technique was used to extract silica particles from pumice rock, which were subsequently modified with iron to enhance their affinity for fluoride. To assess its efficacy, selected borehole water samples were used. Scanning electron microscopy, X-ray diffraction, Fourier transform infrared and X-ray fluorescence spectroscopy was used to characterize the sorbent. The extracted silica particles were 96.71% pure and amorphous, whereas the iron-functionalized silica particles contained 93.67% SiO₂ and 2.93% Fe₂O₃. The optimal pH, sorbent dose and contact time for defluoridation of a 20 mg/L initial fluoride solution were 6, 1 g and 45 min, respectively. Defluoridation followed pseudo-second-order kinetics and fitted Freundlich's isotherm. Fluoride levels in borehole water decreased dramatically; Intex 4.57–1.13, Kadokoi 2.46–0.54 and Naudo 5.39–1.2 mg/L, indicating that the silica-based sorbent developed from low-cost, abundant and locally available pumice rock is efficient for defluoridation.

Groundwater is the most readily accessible source of drinking water, yet it is also the most polluted^{1,2}. Fluoride is one of these pollutants, although at low levels it is also essential in the body as a trace element for the development of teeth and bones^{3,4}. Prolonged exposure to high fluoride levels can cause dental and skeletal fluorosis, as well as harm to the kidneys, liver, brain and thyroid glands^{5,6}. Over 260 million people worldwide are exposed to high fluoride levels through groundwater in the East Africa's Rift Valley, Asia, Europe and America^{7–9}. This has been attributed to geogenic processes such as volcanic activities and weathering of fluoride-rich minerals^{10,11}. Fluoride enrichment in groundwater is also aided by effluents from the fertilizer, ceramic, pesticide, glass, aluminium and refrigerant industries^{12–14}. Today, the World Health Organization (WHO) has established the allowable limit of fluoride in drinking water at 1.5 mg/L¹⁵, hence defluoridation processes such as ion exchange, adsorption, coagulation, precipitation and reverse osmosis are crucial to maintaining fluoride levels within this range^{12,16}. However, the majority of these techniques are expensive to maintain and operate. Another constraint is the production of toxic sludge through methods such as precipitation, coagulation, and membrane filtration. Furthermore, techniques such as reverse osmosis and ion exchange are complicated and expensive, necessitating the use of water adsorbents^{17,18}. Adsorption is the most preferred water purification technique because it is cheap, efficient, does not generate sludge, is simple to operate, and does not need electric power or specialized skills to operate. In addition, the adsorbents can be regenerated and reused making them the best at the household level and in small communities in less developed rural areas¹⁹. Commercial activated carbon derived from coal is among the most effective adsorbent for fluoride removal from water. It has a high specific surface area and is highly porous, however it is extremely expensive and has regeneration difficulties¹⁷. Other effective materials include bauxite²⁰, bone char, metal oxides, polymer materials, biosorbents²¹, agricultural wastes⁶, sea materials, fly ash, carbonaceous materials²², nanoparticles²³ and geomaterials²⁴, all of which are low in cost and readily available, as is the case of silica mineral (SiO₂). Silica is an auspicious materials with distinct features that satisfy almost all of the selection criteria for ideal water purification adsorbents, such as chemical inertness, structural and thermal stability, high specific surface area, non-toxicity, large pore size and the presence of surface functional groups (–Si–OH and –Si–O–Si–) that are readily modified to enhance selectivity towards a target pollutant²⁵. Furthermore, it is abundant and widely distributed in nature, particularly in volcanic rocks such as pumice (60–70%)^{26,27}. It is abundant in Kenya along the Rift Valley System in volcanic centers such as the Barrier, Namanuru, Emuruangogolak, Silali, Paka, Korosi, Menengai, Longonot, and Suswa craters²⁸. Mourhly

Department of Chemistry, School of Mathematics and Physical Sciences, Jomo Kenyatta University of Agriculture and Technology, P.O Box 62000-00200, Nairobi, Kenya. email: paulprono2007@yahoo.com